Stem Cell Reports
Article

ISSCR

OPEN ACCESS

Long noncoding RNA *Lnc530* localizes on R-loops and regulates R-loop formation and genomic stability in mouse embryonic stem cells

Daohua Gong,[1,3,5] Lin Wang,[1,5] Hu Zhou,[2] Jing Gao,[2] Weidao Zhang,[1,5] and Ping Zheng[1,4,5,*]

[1]State Key Laboratory of Genetic Resources and Evolution, Kunming Institute of Zoology, Chinese Academy of Sciences, Kunming, Yunnan 650203, China
[2]Department of Analytical Chemistry and CAS Key Laboratory of Receptor Research, Shanghai Institute of Materia Medica, Chinese Academy of Sciences, Shanghai 201203, China
[3]University of Chinese Academy of Sciences, Beijing 101408, China
[4]KIZ/CUHK Joint Laboratory of Bioresources and Molecular Research in Common Diseases, Kunming Institute of Zoology, Chinese Academy of Sciences, Kunming, Yunnan 650203, China
[5]Key Laboratory of Animal Models and Human Disease Mechanisms of Yunnan Province, Kunming Institute of Zoology, Chinese Academy of Sciences, Kunming, Yunnan 650203, China
*Correspondence: zhengp@mail.kiz.ac.cn
https://doi.org/10.1016/j.stemcr.2023.02.003

SUMMARY

Embryonic stem cells (ESCs) are superior to differentiated cells to maintain genome stability, but the underlying mechanisms remain largely elusive. R-loops are constantly formed during transcription and are inducers of DNA damage if not resolved. Here we report that mouse ESCs (mESCs) can efficiently prevent unscheduled R-loop formation, and a long noncoding RNA *Lnc530* plays regulatory role. *Lnc530* is expressed in mESCs and localizes on R-loops. Depletion of *Lnc530* in mESCs causes R-loop accumulation and DNA damage, whereas forced expression of *Lnc530* in differentiated cells suppresses the R-loop formation. Mechanistically, *Lnc530* associates with DDX5 and TDP-43 in an inter-dependent manner on R-loops. Formation of *Lnc530*-DDX5-TDP-43 complex substantially increases the local protein levels of DDX5 and TDP-43, both of which play critical roles in R-loop regulation. This study uncovers an efficient strategy to prevent R-loop accumulation and preserve genomic stability in mESCs and possibly other stem cell types.

INTRODUCTION

Embryonic stem cells (ESCs) are derived from the inner cell mass of blastocysts. Due to the characteristics of pluripotency and self-renewal, ESCs are widely utilized in basic research and have promising applications in cell-based regenerative medicine (Kimbrel and Lanza, 2015; Takahashi and Yamanaka, 2016). Aside from the property of pluripotency, ESCs have super-stable genome, which is crucial for the maintenance of stem cell identity (Maynard et al., 2008). Previous studies compared the genome mutation rates of mouse ESCs (mESCs) with their isogenic mouse embryonic fibroblasts (MEFs), and found that the mutation rate of mESCs was 100 times lower than that of MEFs (Cervantes et al., 2002; Tichy and Stambrook, 2008). Although some pioneer works revealed that the mESC-specific mechanisms play essential roles to ensure efficient genome stability regulation (Wang et al., 2021; Xiong et al., 2015; Zhang et al., 2019; Zhao et al., 2015, 2018), how mESCs maintain the genome stability during the rapid self-renewal remains largely unclear. Investigating the underlying mechanisms would expand the knowledge and provide clues to develop strategies to improve the safety of stem cell applications (Andrews et al., 2022).

R-loops are transient structures consisting of a DNA-RNA hybrid and a displaced single-stranded DNA (ssDNA) (Li and Manley, 2005; Sanz et al., 2016). R-loops (regulatory or unscheduled) can form co-transcriptionally when the nascent RNA hybridizes with the template DNA (Aguilera and Garcia-Muse, 2012). Distinct from the short form of RNA-DNA hybrid formed during transcription and lagging-strand DNA replication, R-loops generally span for 100–2,000 base pairs and play double-edged roles in many cellular activities (Costantino and Koshland, 2015). Regulatory R-loops are essential in a number of physiological processes, including transcription regulation (Skourti-Stathaki and Proudfoot, 2014), immunoglobulin class switching (Bhatia et al., 2017), homologous recombination (HR)-mediated DNA damage repair (Ohle et al., 2016; Yasuhara et al., 2018), telomere lengthening (Arora et al., 2014; Balk et al., 2013), and epigenetic modification of chromatin (Castellano-Pozo et al., 2013; Skourti-Stathaki et al., 2014). However, unscheduled or aberrant R-loops represent a major threat to genome stability. They can induce transcription stress and generate transcription-associated genomic instability (Aguilera and Gomez-Gonzalez, 2017; Hamperl and Cimprich, 2016). Moreover, R-loops can also be recognized by several nucleases and converted into DNA breaks (Sollier et al., 2014). In mitotic cells, R-loops could be a roadblock to DNA replication (Garcia-Muse and Aguilera, 2019). When the DNA replication fork encounters transcription machinery in the head-on orientation, the transcription-replication collisions (TRCs) stall transcription and induce persistent R-loop

This is an open access article under the CC BY-NC-ND license (http://creativecommons.org/licenses/by-nc-nd/4.0/).

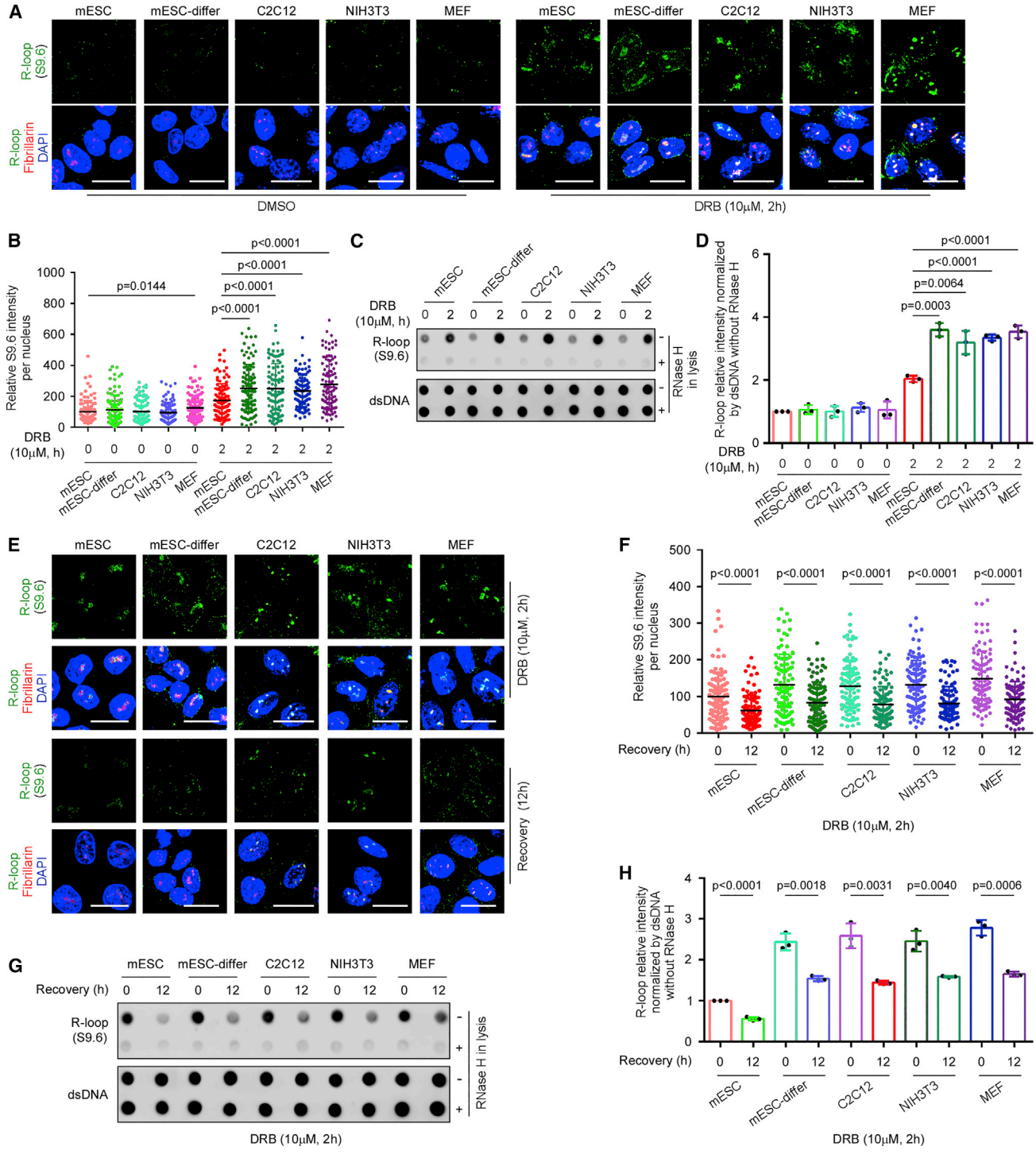

Figure 1. mESCs have high efficiency to prevent R-loop formation

(A) Immunostaining detection of R-loops in mESC, mESC-differentiated cells (mESC-differ), C2C12, NIH3T3, and MEFs. R-loop was labeled by S9.6 (green), and nucleolus was labeled by fibrillarin (red). Scale bars, 20 μm. See also Figure S1.

(B) Quantification of S9.6 staining intensity in (A). At least 20 visual fields containing 500 cells were analyzed in three independent experiments.

(C and D) Detection (C) and quantification (D) of R-loops by dot blotting of genomic DNA from the mESCs and differentiated cells. Double-stranded DNA (dsDNA) was used as internal reference.

(legend continued on next page)

formation. R-loops conversely block replication and transcription, cause potential replication stress-associated DNA damage (Hamperl et al., 2017; Kim et al., 2020; Sankar et al., 2016), and impair self-renewal (Abakir et al., 2020; Pappa et al., 2019). Thus, R-loop formation and resolution must be carefully regulated to avoid aberrant R-loop accumulation.

To protect the genome from excessive R-loop accumulation, cells deploy different mechanisms to prevent R-loop formation and to resolve existing R-loops. By utilizing DNA-RNA immunoprecipitation (DRIP) or proximity labeling combined with mass spectrometry (MS) analyses, previous studies have identified the interactome of R-loops (Wang et al., 2018; Yan et al., 2022). Several hundreds of proteins have been identified, and the largest category is the RNA-DNA helicases, particularly DEAD (Asp-Glu-Ala-Asp) or DEAH (Asp-Glu-Ala-His)-box members, whose mutations affect the formation and resolution of R-loops (Bjorkman et al., 2020; Frame and North, 2021; Grunseich et al., 2018) and are associated with human diseases including amyotrophic lateral sclerosis (ALS) and frontotemporal dementia (FTD) (Skourti-Stathaki and Proudfoot, 2014; Walker et al., 2017; Wang et al., 2018). RNase H is also key to R-loop resolution *in vivo* (Cerritelli and Crouch, 2009), and deficiency of the enzyme causes a severe neuroinflammatory disease, Aicardi Goutières syndrome (AGS) (Cristini et al., 2022). In addition, other factors that facilitate the RNA processing or alter the DNA topology can affect R-loop formation and resolution (Luo et al., 2022; Stolz et al., 2019). Telomeric-repeat-containing RNA (TERRA) preferentially associates with short telomeres through the formation of telomeric R-loop structures to regulate telomeric chromatin structure and suppress DNA damage (Feretzaki et al., 2020; Vohhodina et al., 2021).

ESCs proliferate rapidly (e.g., 10–12 h per cell cycle in mESCs). The frequent DNA replication increases the chance of TRCs and enhances the opportunity to form undesirable R-loops. However, the genome of mESCs remains super-stable, raising the hypothesis that mESCs might be able to efficiently prevent undesirable R-loop formation or accumulation. In this study, we reported that an mESC-expressed long noncoding RNA (lncRNA), *Lnc530*, played essential roles in preventing R-loop accumulation. *Lnc530* associated with DDX5 and TDP-43, two R-loop regulators, on R-loops and increased their local protein levels to enhance R-loop regulation and genomic stability.

RESULTS

mESCs are able to efficiently prevent R-loop formation

To investigate whether mESCs can prevent R-loop accumulation with higher efficiency, we utilized the reversible transcription inhibitor 5,6-dichloro-1-β-*d*-ribofuranosylbenzimidazole (DRB) to induce R-loop formation (Scalera et al., 2021) in mESCs and several types of differentiated cells, including MEFs, NIH3T3, mouse myoblasts C2C12, and isogenic mESC-differentiated cells (mESC-differ) cultured in medium depleted of LIF (Figure S1A). R-loop formation was detected by immunofluorescent staining with S9.6 antibody, which specifically recognizes the DNA-RNA hybrids (Boguslawski et al., 1986; Bou-Nader et al., 2022). Treatment with DRB for 2 h induced a lower level of R-loops in mESCs than in all types of differentiated cells (Figures 1A and 1B). R-loop levels were also assessed by dot blotting of nuclear DNA with S9.6 antibody, and a consistent result was obtained (Figures 1C and 1D). To rule out the possibility that mESCs display lower transcriptional activity that contributes to less R-loop formation, we compared the transcriptional activity among these cell types. Nascent RNAs were labeled with uridine analog 5-ethynyluridine (EU) for 30 min (Kim et al., 2020) and were detected by immunofluorescent staining. As shown (Figure S1B), the transcriptional activity in mESCs was comparable with or even higher than that in all the differentiated cells. Thus, mESCs were more efficient than differentiated cells to prevent aberrant R-loop formation. We then washed away the DRB and investigated the resolution of existing R-loops in mESCs and differentiated cells. The immunofluorescence and dot-blot analyses consistently showed that the resolution rates of existing R-loops did not differ between mESCs and differentiated cells (Figures 1E–1H). Taken together, these observations suggested that mESCs, compared with the differentiated cells, could efficiently prevent R-loop formation.

mESC-expressed lncRNA *Lnc530* prevents R-loop accumulation and DNA damage

We previously identified an uncharacterized lncRNA NONMMUT019530 (NONCODE ID, *Lnc530* for short) in studying the regulation of genomic stability in mESCs. *Lnc530* was expressed in mESCs at a higher level compared with several differentiated cell types, including isogenic mESC-differentiated cells (Figure S2A). The expression of *Lnc530* also decreased in the process of mESC

(E and F) Dynamics of R-loop resolution. Representative images (E) and quantification (F) of S9.6 staining intensity per nucleus in mESCs and differentiated cells. At least 20 visual fields containing 500 cells were analyzed in three independent experiments. Scale bars, 20 μm. (G and H) (G) Dot-blot analysis showed the similar kinetics of R-loop resolution in mESCs and differentiated cells. (H) The quantification of dot blot intensity. dsDNA was internal reference. All experiments were repeated three times with similar results. Data are shown as mean ± SD, two-tailed Student's t test.

differentiation via embryoid body (EB) formation (Figure S2B). Intriguingly, some regions of mouse brain expressed higher levels of *Lnc530* than mESCs (Figure S2C). These expression patterns indicated that *Lnc530* might function in mESCs and brain. Based on mouse reference genome assembly version mm10, the *Lnc530* gene has two genomic copies and is located on the plus strand of chromosome 14 (Figure S2D). Full-length (FL) analysis by 3′- and 5′-end rapid amplification of cDNA ends (RACE) showed that it contained two exons and had two isoforms (long and short isoforms) (Figure S2E). Because no suitable primer was available to distinguish the expression of two isoforms of *Lnc530* by quantitative RT-PCR, we were unable to know their relative abundance. Although *Lnc530* transcripts contain one potential coding frame, *in vitro* translation assay failed to detect any translation of protein or peptide (Figure S2F). Thus, *Lnc530* is a potential noncoding RNA, and the sequences of two isoforms are listed in Figures S3A and S3B.

To investigate whether *Lnc530* plays role in regulating genomic stability of mESCs, we designed two independent doxycycline (Dox)-inducible short hairpin RNAs (shRNAs), which targeted both isoforms (Figure S3C). *Lnc530* was efficiently knocked down by two shRNAs in mESCs (Figure S3C). Depletion of *Lnc530* induced DNA double-strand breaks (DSBs), monitored by γH2AX accumulation (Figures 2A and 2B) and comet tail lengthening in neutral comet assay (Figure 2C). DSB generation is often associated with other forms of genomic instability. Concordantly, *Lnc530* knockdown (KD) mESCs displayed higher rates of micronuclei (Figure 2D) and aneuploidy (Figure 2E). Because genomic instability can impair mESC self-renewal, we examined the influence of *Lnc530* KD on ESC proliferation as well as pluripotency marker expressions. Mitotic cells were labeled by thymidine analog 5-Ethynyl-2′-deoxyuridine (EdU), and flow cytometry analysis showed that *Lnc530* KD impaired mESC proliferation (Figure 2F). However, the pluripotency marker expressions were not affected, and *Lnc530* KD mESCs displayed normal colony morphology (Figure 2G).

To understand how *Lnc530* regulates the genomic stability in mESCs, we first examined its subcellular localization by fluorescence *in situ* hybridization (FISH). Intriguingly, *Lnc530* localized on R-loops after DRB treatment in mESCs, whereas its distribution on R-loops was not obviously detected in differentiated cells (Figure 3A). This observation implicated a potential role of *Lnc530* in regulating R-loops to ensure genomic stability in mESCs. We thus investigated the influence of *Lnc530* KD on R-loop accumulation. Immunostaining with S9.6 antibody revealed that *Lnc530* KD mESCs contained a higher level of R-loops than KD control ESCs under normal culture conditions (Figures 3B and 3C). The increase in R-loop accumulation after *Lnc530* KD was further validated by dot-blot analysis (Figures 3D and 3E). R-loops consist of displaced ssDNA. Concordantly, thymidine analog 5-Chloro-2′-deoxyuridine (CIdU) labeling under the natural condition detected an increased level of ssDNA in *Lnc530* KD mESCs (Figures 3F and 3G). We also over-expressed FLAG-tagged RNase H1, which resolves R-loops, in *Lnc530* KD cells (Figure S3D). The increases in R-loop accumulation and ssDNA formation were counteracted by over-expression of RNase H1 in *Lnc530* KD mESCs (Figures 3B–3G), again supporting the regulation of *Lnc530* on R-loops. Because aberrant R-loop accumulation induces DNA damage and genomic instability, we proposed that *Lnc530* localized on R-loops to prevent R-loop accumulation and preserve genomic stability in mESCs.

Lnc530 associates with DDX5 and TDP-43 in an interdependent manner

To understand how *Lnc530* regulates R-loops, we performed *in vivo* RNA pull-down combined with MS analysis to identify the potential interaction proteins of *Lnc530*. MS analysis of *in vivo* pull-down samples reproducibly identified a list of binding candidates in two replicates (Table S1). Among these candidates, DDX5 and TDP-43 (also known as TARDBP) were previously reported to associate with and regulate R-loops (Giannini et al., 2020; Le et al., 2021; Mersaoui et al., 2019; Wood et al., 2020). We then focused on the two proteins and validated their interaction with *Lnc530*. *In vivo* cross-linking followed by nucleus-cytoplasm fractionation and RNA pull-down showed that *Lnc530* was associated with DDX5 and TDP-43 in the nucleus. Induction of R-loops by DRB or hydroxylurea (HU) treatment drastically enhanced their interaction. However, no visible interaction was detected in cytoplasm under the normal culture or drug treatment conditions (Figure 4A). Thus, *Lnc530* can interact with DDX5 and TDP-43 in the nucleus of mESCs.

We next asked whether *Lnc530*-DDX5-TDP-43 associated with each other. To this end, we performed reciprocal immunoprecipitation (IP). DDX5 physically interacted with TDP-43, and their association was enhanced by R-loop induction (Figures 4B and 4C). Notably, DDX5-TDP-43 interaction was significantly decreased by *Lnc530* KD (Figures 4B and 4C), suggesting that the DDX5-TDP-43 association requires *Lnc530*. We also depleted DDX5 by Dox-inducible shRNA (Figure S3E) and examined its influence on TDP-43 and *Lnc530*. DDX5 KD did not affect the expression of TDP-43 or *Lnc530* (Figures S3F and S3G). However, it attenuated *Lnc530*-TDP-43 interaction, which was successfully restored by re-expression of FLAG-tagged DDX5 in KD cells (Figures 4D and S3E). Similarly, depletion of TDP-43 reduced the *Lnc530*-DDX5 interaction, and re-expression of FLAG-tagged TDP-43 rescued the defect

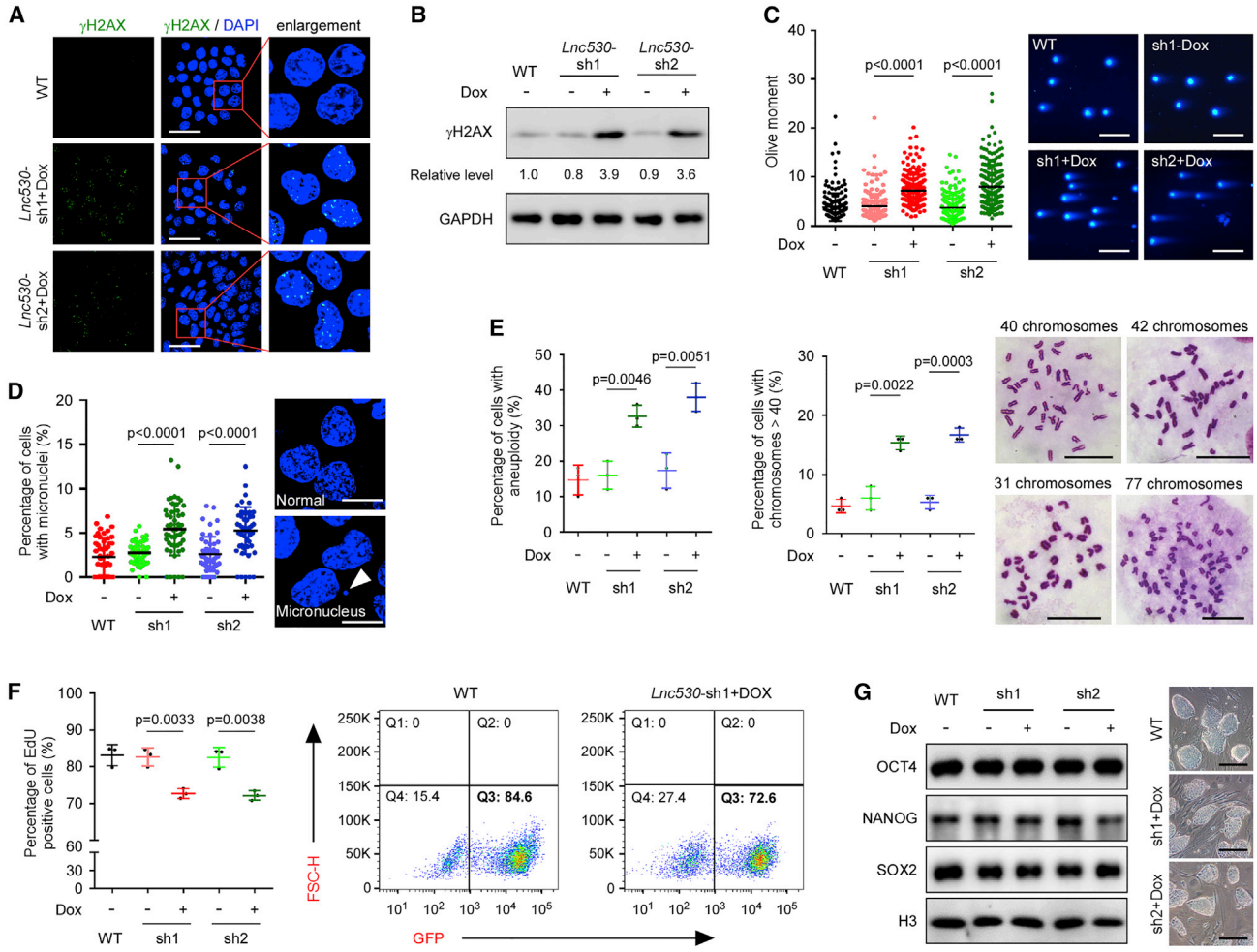

Figure 2. Loss of *Lnc530* causes genomic instability in mESCs

(A and B) Immunostaining (A) and immunoblotting (B) showed that depletion of *Lnc530* increased DSB formation as monitored by increased γH2AX level. Scale bars, 40 μm.

(C) Neutral comet assay validated the increased DSB level in *Lnc530* KD mESCs. Left panel shows the quantification of comet tail length. Right panel shows representative images. At least 200 tails were analyzed in each group. Scale bars, 400 μm.

(D) More *Lnc530* KD mESCs contained micronuclei. Left panel shows the quantification of micronuclei formation. Right panel shows representative images (arrow). At least 50 visual fields containing 1,000 cells were analyzed in each group. Scale bars, 10 μm.

(E) More *Lnc530* KD mESCs displayed aneuploidy. Left panel shows the quantification of aneuploidy. Middle panel shows the quantification of aneuploidy with chromosome numbers >40. Right panel shows representative images. At least 150 metaphase spreads were examined in three replications in each group. Scale bars, 20 μm.

(F) Flow cytometry assay showed that the proliferation of *Lnc530* KD mESCs was impaired. Left panel shows the quantification result. Right panel shows representative images of flow cytometry.

(G) Immunoblotting showed that the protein expression of core pluripotency regulators SOX2, NANOG, and OCT4 was not changed in *Lnc530* KD mESCs (left). Moreover, *Lnc530* KD mESCs had normal colony morphology (right). Scale bars, 200 μm. All experiments were independently repeated three times with similar results. The relative protein levels in (B) were normalized by GAPDH. Data are shown as mean ± SD, two-tailed Student's t test.

(Figures 4E and S3H). Altogether, these data demonstrate that *Lnc530*-DDX5-TDP-43 form a complex in an interdependent manner.

To provide more details on their interaction, we went on to map the TDP-43-DDX5 binding sites on *Lnc530*. The CatRAPID online tool (Armaos et al., 2021; Ribeiro et al., 2018) predicted that the two proteins had same putative binding sites on *Lnc530*, which locate at the fragments of 2,395–2,522 base pair (bp) and 2,899–3,026 bp. We then generated a series of *Lnc530* truncates including

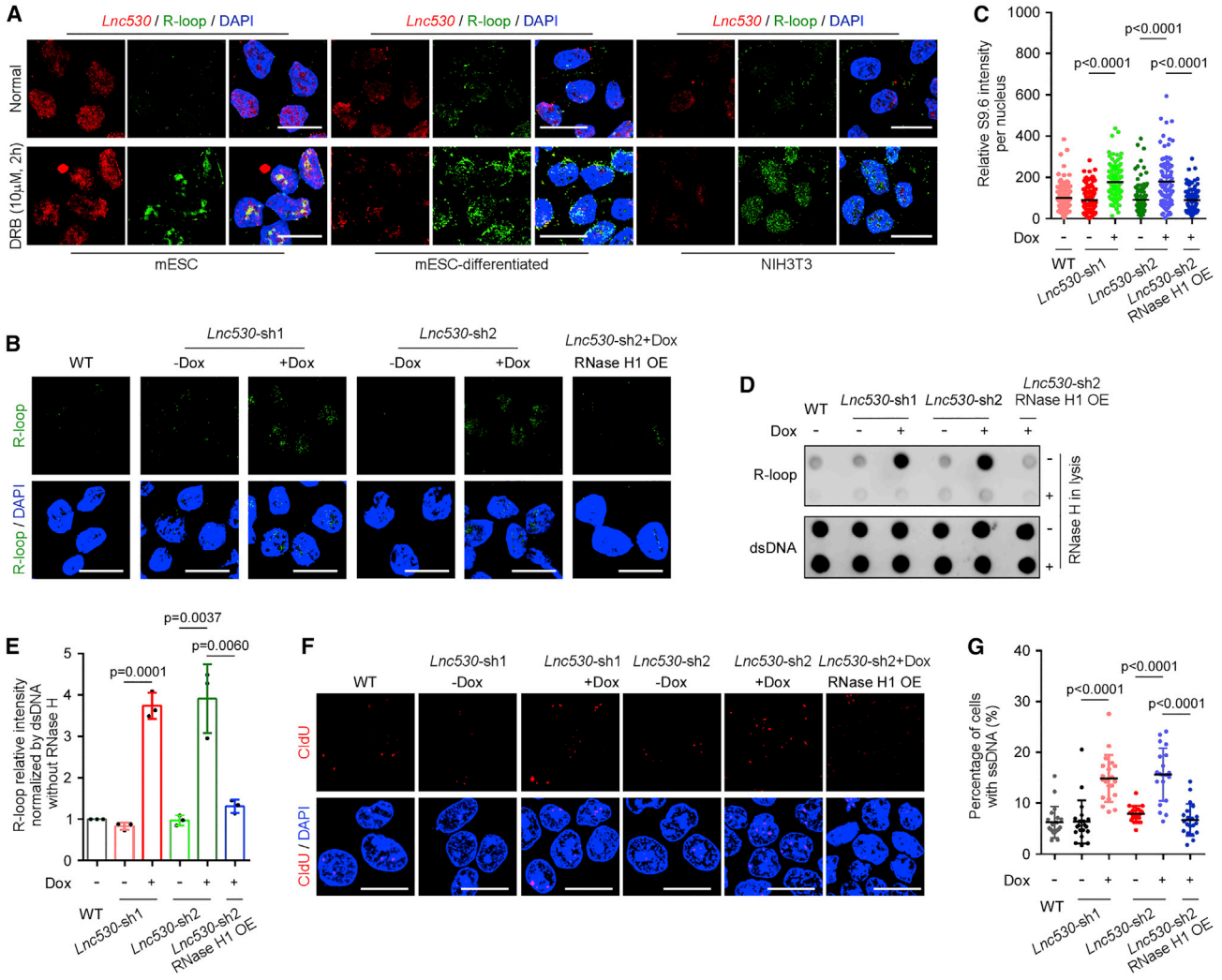

Figure 3. Loss of *Lnc530* perturbs R-loop homeostasis

(A) Immunostaining and RNA-FISH show that *Lnc530* was localized on R-loops in mESCs rather than in differentiated cells after DRB treatment. Scale bars, 20 μm.

(B and C) Representative images (B) and quantification (C) of S9.6 staining in mESCs. *Lnc530* KD increased the R-loop level in mESCs. At least 20 visual field containing 500 cells were analyzed in three independent experiments. Scale bars, 20 μm.

(D and E) Dot-blot analysis (D) showed that R-loop level were increased in *Lnc530* KD mESCs. The quantification of dot blot intensity is shown in (E). dsDNA was internal reference.

(F and G) Immunostaining (F) and quantification (G) of ssDNA signal in mESCs. ssDNA was monitored by CIdU (red). *Lnc530* KD increased the level of ssDNA in mESCs. At least 20 visual fields containing 1,000 cells were analyzed in each group. Scale bars, 20 μm. All experiments were independently repeated three times with similar results. Data are shown as mean ± SD, two-tailed Student's t test.

Δ2,301–3,172 (deletion of 2,301–3,172), Δ1–2,300 (deletion of 1–2,300), Δ2,301–2,600 (deletion of 2,301–2,600), and Δ2,601–3,172 (deletion of 2,601–3,172) (Figure 4F). *In vitro* RNA pull-down assay revealed that, compared with the FL *Lnc530* (long isoform), Δ2,301–3,172 failed to pull down TDP-43 and DDX5, whereas Δ1–2,300 displayed normal pull-down efficiency. Notably, two truncates, Δ2,301–2,600 and Δ2,601–3,172, which lack either one of the two predicted binding sites, showed reduced ability to interact with TDP-43 and DDX5 (Figure 4F). These results suggested that the DDX5-TDP-43 protein complex bound to the sites located within 2,301–2,600 and 2,601–3,172 in *Lnc530*.

TDP-43 is an RNA-binding protein containing two RNA recognition motifs (RRMs), RRM1 and RRM2 (Buratti and Baralle, 2001; D'Ambrogio et al., 2009). The online tool catRAPID predicted that *Lnc530* might interact with RRM1 of TDP-43. To test this hypothesis, we generated

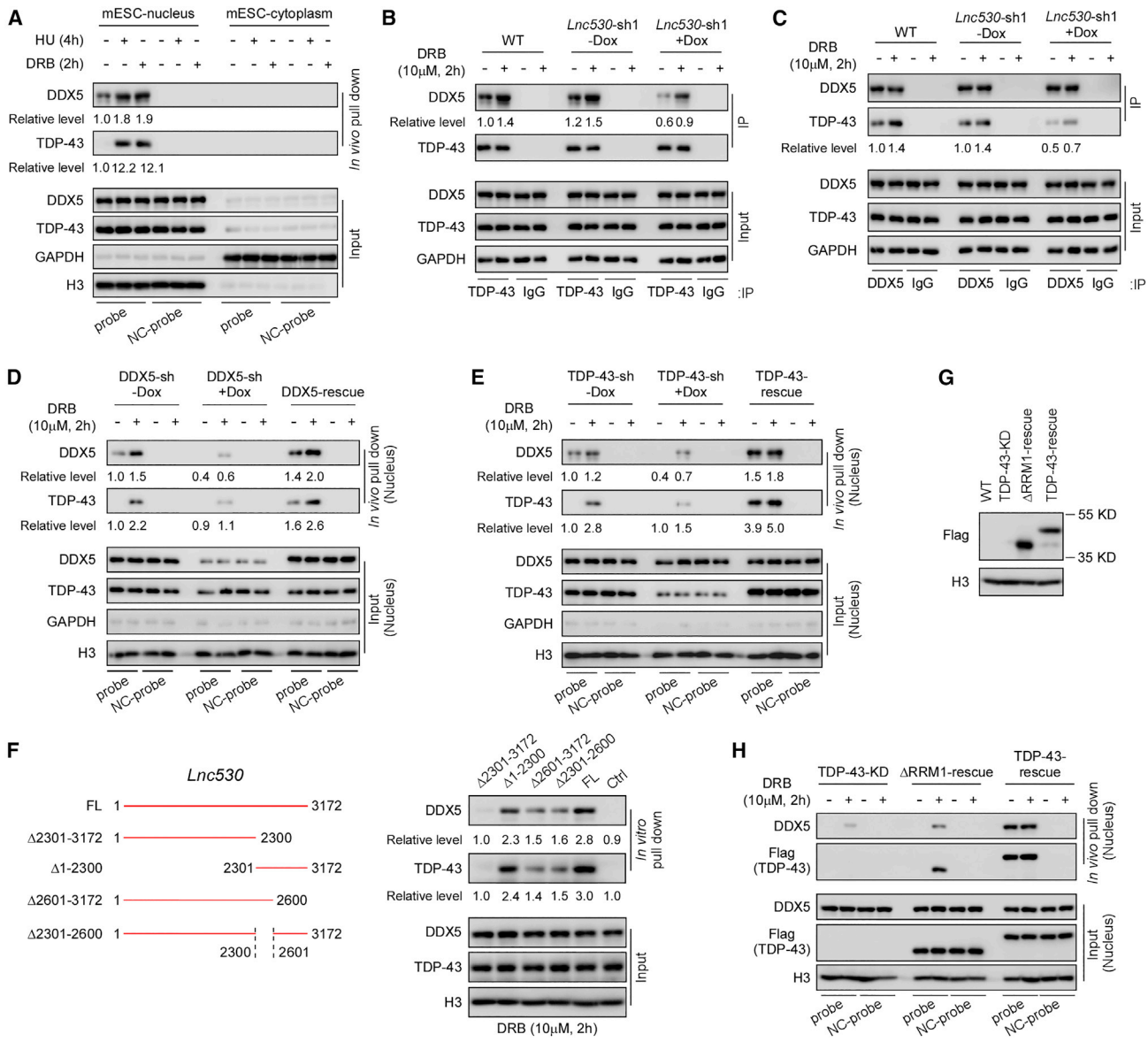

Figure 4. *Lnc530*-TDP-43-DDX5 form a complex under transcription stress condition

(A) mESCs were fractionated into compartments of cytoplasm and nucleus. *In vivo* RNA pull-down assay detected the association of *Lnc530* with TDP-43 and DDX5 in nucleus. NC-probe, negative control probe.

(B and C) Reciprocal immunoprecipitation (IP) showed that DDX5 and TDP-43 associated with each other and the interaction was impaired in *Lnc530* KD mESCs.

(D–F) (D) *In vivo* RNA pull-down assay showed that *Lnc530*-TDP-43 association was impaired in DDX5 KD mESCs. Re-expression of DDX5 (DDX5-rescue) restored the interaction. NC-probe, negative control probe. See also Figure S3 (E) *In vivo* RNA pull-down showed that *Lnc530*-DDX5 association was impaired in TDP-43 KD mESCs. Re-expression of TDP-43 (TDP-43-rescue) restored the interaction. NC-probe, negative control probe. See also Figure S3 (F) *In vitro* RNA pull-down using full-length (FL) and variable truncated *Lnc530* revealed the fragments in *Lnc530* responsible for binding to TDP-43/DDX5. Anti-sense *Lnc530* was used as control (Ctrl).

(G) Immunoblotting confirmed the expression of TDP-43-ΔRRM1 (ΔRRM1-rescue) and WT TDP-43 (TDP-43-rescue) in TDP-43 KD mESCs.

(H) *In vivo* RNA pull-down assay revealed that *Lnc530* could not interact with TDP-43-ΔRRM1 mutant protein. NC-probe, negative control probe. All experiments were independently repeated three times with similar results. The relative protein levels in (A)–(F)) were normalized by input.

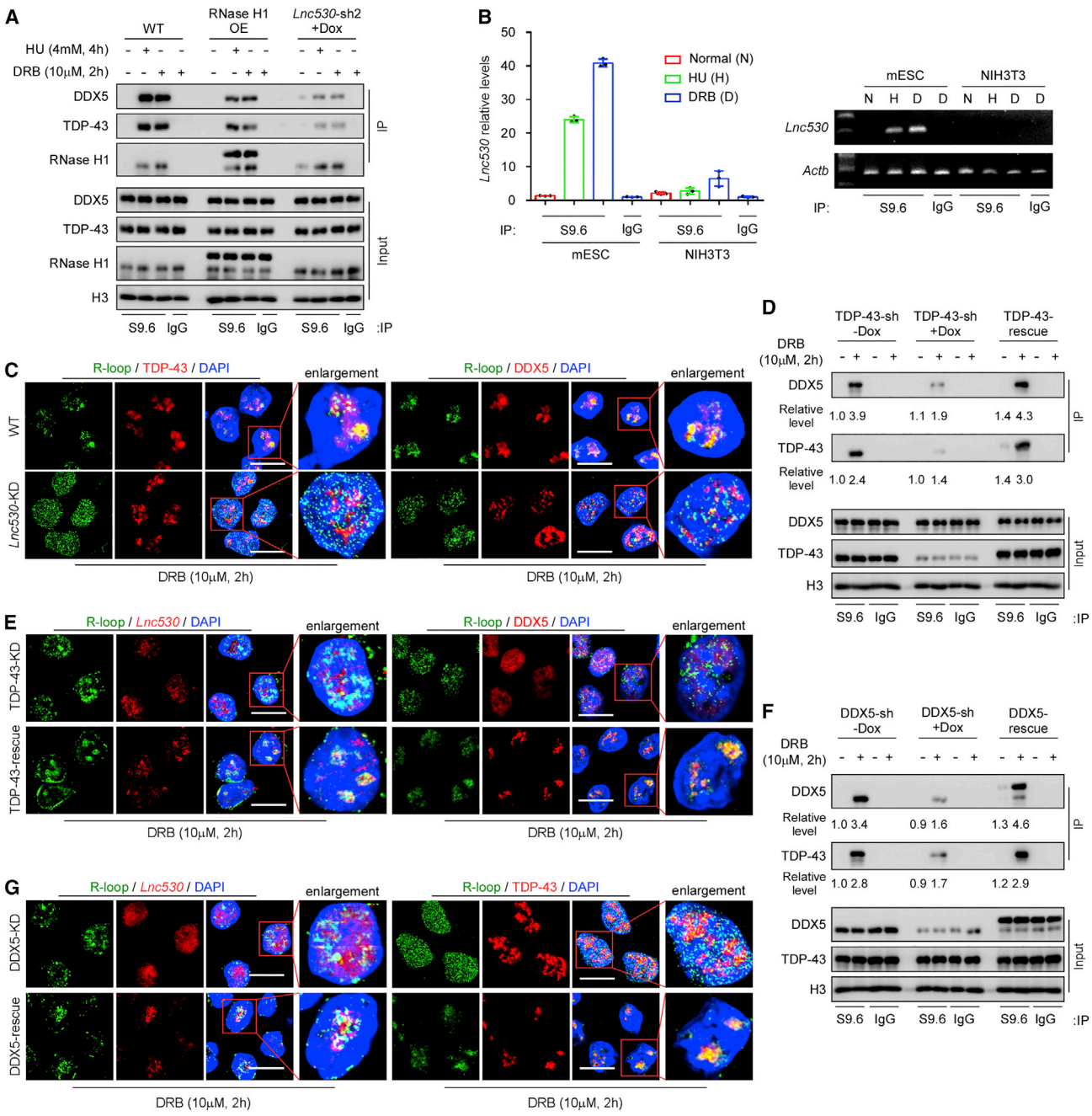

Figure 5. *Lnc530*-TDP-43-DDX5 complex is localized on R-loop under transcription stress condition

(A) S9.6 IP showed that TDP-43 and DDX5 were accumulated on R-loops in mESCs under transcription stress condition. RNase H1 overexpression (OE) or *Lnc530* KD reduced the accumulation of TDP-43 and DDX5 on R-loops.

(B) S9.6 IP combined with RT-qPCR analysis for detection of *Lnc530* on R-loops in mESCs and NIH3T3. Left panel shows the relative levels of *Lnc530*. Right panel shows the RT-PCR bands. *Actb* was set as internal reference.

(C) Immunostaining showed that *Lnc530* KD impaired the accumulation of TDP-43 (left) or DDX5 (right) on R-loops. Scale bars, 20 μm.

(D) S9.6 IP showed that TDP-43 KD impaired the allocation of DDX5 on R-loops. Re-expression of TDP-43 (TDP-43-rescue) rescued the defect.

(E) Immunostaining showed that accumulation of *Lnc530* (left) or DDX5 (right) on R-loops was impaired in TDP-43 KD mESCs. Re-expression of TDP-43 (TDP-43-rescue) rescued the defect. Scale bars, 20 μm.

(legend continued on next page)

FLAG-tagged ΔRRM1 mutation (deletion of 106–175 amino acids) and re-expressed the mutant protein in TDP-43 KD mESCs (Figure 4G). *In vivo* RNA pull-down assay revealed that ΔRRM1 compromised the interaction of *Lnc530* with DDX5 and TDP-43 (Figure 4H), indicating that RRM1 motif in TDP-43 was involved in mediating the interaction of *Lnc530* with the DDX5-TDP-43 protein complex.

Lnc530-DDX5-TDP-43 complex localizes on R-loops as a whole

Next, we examined whether the *Lnc530*-DDX5-TDP-43 complex localized on R-loops in mESCs. R-loops were enriched by IP with S9.6 antibody. After treatment with DRB or HU to stimulate R-loop formation in mESCs, we detected the robust accumulation of DDX5, TDP-43, and *Lnc530* on R-loops (Figures 5A and 5B). Forced expression of FLAG-tagged RNase H1 in wild-type (WT) mESCs (Figure S4A) concordantly decreased the levels of DDX5 and TDP-43 in precipitates (Figure 5A).

Because *Lnc530*-DDX5-TDP-43 form a complex in an inter-dependent manner, we speculated that depletion of each component influenced the recruitment of other components to R-loops. Under DRB treatment conditions, *Lnc530* KD mESCs contained more R-loops (Figures S4B and S4C). However, significantly less DDX5 and TDP-43 were co-immunoprecipitated with R-loops in *Lnc530* KD mESCs under HU or DRB treatment conditions (Figure 5A). Because *Lnc530* KD did not affect the protein expression of DDX5 and TDP-43 (Figure S4D), this result suggested that the allocation of DDX5 and TDP-43 on R-loops was impaired by *Lnc530* KD. Consistently, immunostaining validated the reduced localization of the two proteins on R-loops in *Lnc530* KD mESCs (Figure 5C). Similar to *Lnc530* KD, depletion of TDP-43 compromised the allocation of DDX5 and *Lnc530* on R-loops, and re-expression of TDP-43 rescued the phenotypes (Figures 5D and 5E). The accumulation of TDP-43 and *Lnc530* on R-loops was also reduced or recovered when DDX5 was depleted or re-expressed, respectively (Figures 5F and 5G). Thus, these data altogether support that the *Lnc530*-DDX5-TDP-43 complex is associated with R-loops.

DDX5 and TDP-43 mediate the regulation of *Lnc530* on R-loops

DDX5 and TDP-43 can regulate R-loops in differentiated cells (Giannini et al., 2020; Le et al., 2021; Mersaoui et al., 2019; Wood et al., 2020). We wondered whether DDX5 and TDP-43 played conserved roles in the context of mESCs. Immunostaining showed that, under normal culture conditions, KD of DDX5 or TDP-43 induced R-loop accumulation, which was alleviated by over-expression of FLAG-tagged RNase H1 (Figure S5A) or re-introduction of respective protein (Figures 6A and 6B). Consistent results were obtained by dot-blot analysis of chromatin (Figures 6C and 6D). We also examined the amount of displaced ssDNA in R-loops. Accompanying the induction of DNA-RNA hybrids, a large amount of ssDNA appeared in DDX5 KD and TDP-43 KD mESCs, respectively. Over-expression of RNase H1 or re-expression of respective protein decreased the ssDNA level (Figures 6E and 6F). Concordantly, DDX5 KD or TDP-43 KD mESCs contained higher levels of DNA DSBs (Figure 6G), micronuclei (Figure 6H), and aneuploidy (Figure 6I). The DNA DSB defect was rescued by over-expression of RNase H1 or respective protein (Figure 6G). These results suggest that DDX5 and TDP-43 prevent R-loop accumulation and mediate the regulatory function of *Lnc530* on R-loops in mESCs.

To further verify the conclusion that DDX5 and TDP-43 mediate the function of *Lnc530*, we over-expressed the FLAG-tagged TDP-43 and DDX5 proteins in *Lnc530* KD mESCs (Figure S5B), and examined whether it rescued the defects caused by *Lnc530* KD. Over-expression of TDP-43 and DDX5 suppressed the R-loop induction caused by *Lnc530* KD under normal culture or DRB treatment conditions, as assessed by immunostaining (Figures S5C and S5D) as well as dot-blot analysis of chromatin (Figure S5E). Similarly, the defects of DNA DSBs (Figure S5F) and micronuclei formation (Figure S5G) in *Lnc530* KD mESCs were rescued by over-expression of TDP-43 and DDX5. However, aneuploidy could not be rescued (Figure S5H). Taken together, these data support that DDX5 and TDP-43 mediate the regulation of *Lnc530* on R-loops.

Ectopic expression of *Lnc530* in differentiated cells reduces the aberrant R-loop formation by increasing the recruitment of DDX5-TDP-43 to R-loops

mESCs express *Lnc530* at higher levels than many types of differentiated cells. *Lnc530* in mESCs promotes the association of *Lnc530*-DDX5-TDP-43 complex with R-loops to prevent the aberrant R-loop accumulation. We wondered whether forced expression of *Lnc530* in differentiated cells could be sufficient to induce *Lnc530*-DDX5-TDP-43 interaction and to increase the recruitment of DDX5-TDP-43

(F) S9.6 IP showed that DDX5 KD impaired the association of TDP-43 with R-loops, which was restored by re-expression of DDX5 (DDX5-rescue).

(G) Immunostaining revealed that accumulation of *Lnc530* (left) and TDP-43 (right) on R-loops was impaired in DDX5 KD mESCs, and the defects were rescued by re-expression of DDX5 (DDX5-rescue). Scale bars, 20 μm. All experiments were independently repeated three times with similar results. The relative protein levels in (D) and (F) were normalized by input.

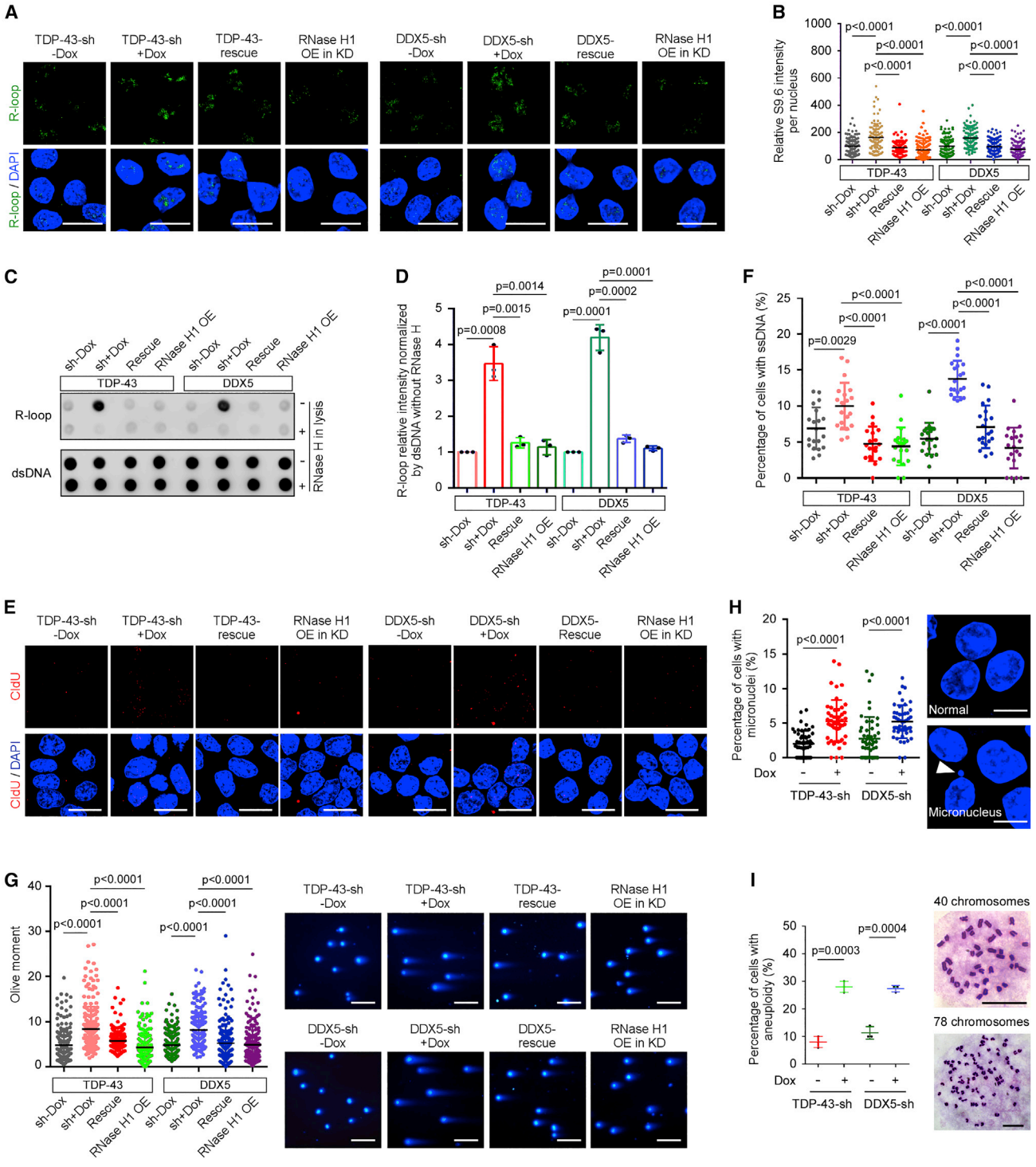

Figure 6. Loss of TDP-43 or DDX5 induces R-loop accumulation and DNA damage

(A) Immunostaining showed that TDP-43 KD or DDX5 KD induced the R-loop formation in mESCs. Re-expression of TDP-43 (TDP-43-rescue), DDX5 (DDX5-rescue), or RNase H1 OE in KD cells rescued the defect. Scale bar, 20 μm.

(B) Quantification of R-loop immunostaining intensity in (A). At least 20 visual fields containing 500 cells were analyzed in three independent experiments.

(legend continued on next page)

to R-loops, leading to enhanced R-loop regulation. To this end, we ectopically expressed FL *Lnc530* in NIH3T3 cells. As a negative control, truncated *Lnc530* Δ2,301–3,172, which could not interact with DDX5-TDP-43, was over-expressed in NIH3T3 cells (Figure S6A). *In vivo* RNA pull-down assay validated the interaction of DDX5-TDP-43 with exogenous FL *Lnc530* under normal culture and treatment conditions (Figure 7A). Reciprocal IP also showed that DDX5-TDP-43 association was stimulated by expression of FL *Lnc530* rather than truncated *Lnc530* Δ2,301–3,172 (Figure 7B). Consequently, more DDX5 and TDP-43 were recruited to R-loops in NIH3T3 cells expressing FL but not truncate *Lnc530* (Figure 7C). These results suggested that ectopic expression of *Lnc530* was sufficient to evoke the assembly of *Lnc530*-DDX5-TDP-43 complex on R-loops in differentiated cells. In line with the increased accumulation of DDX5 and TDP-43 on R-loops, ectopic expression of FL *Lnc530*, but not truncated *Lnc530*, in NIH3T3 cells increased the competence to prevent R-loop formation under HU or DRB treatment conditions, as shown by immunostaining (Figures 7D and 7E) as well as dot-blot analysis (Figures 7F and 7G). Concordantly, neutral comet assay revealed that FL *Lnc530*-expressing NIH3T3 cells contained lower levels of DNA DSBs than WT NIH3T3 cells or NIH3T3 cells expressing truncated *Lnc530* after DRB or HU treatment (Figure 7H).

To further validate the observations, we repeated the experiments in isogenic mESC-differentiated cells. mESCs were differentiated for 14 days as described above. FL *Lnc530* was over-expressed in mESC-differentiated cells (Figure S6B). Consistently, over-expression of *Lnc530* suppressed the R-loop accumulation in isogenic differentiated cells as detected by immunostaining (Figures S6C and S6D) and dot-blot analyses (Figures S6E and S6F). The DNA DSBs level in mESC-differentiated cells was also decreased after over-expression of *Lnc530* (Figure S6G). Taken together, we proposed a working model in which *Lnc530* increases the cellular ability to prevent undesirable R-loop formation by driving the *Lnc530*-DDX5-TDP-43 complex assembly and elevating the local concentrations of DDX5 and TDP-43 to regulate R-loops (Figure 7J).

DISCUSSION

Unscheduled R-loop accumulation can promote DNA damage and chromosome instability. R-loop homeostasis must be tightly regulated to maintain genomic stability. In this study, we reported that mESCs, which possess superior stable genome over differentiated cells, had high capacity to prevent aberrant R-loop formation to avoid R-loop-induced DNA damage. Intriguingly, we found that an mESC-expressed lncRNA *Lnc530* attributed to this capacity. *Lnc530* localizes on R-loops, where it physically interacts with DDX5 and TDP-43, thereby increasing the recruitment of two proteins to R-loops. DDX5 and TDP-43 are two essential R-loop regulators and their increased recruitment to R-loops enhanced the homeostasis regulation of R-loops. *Lnc530*-DDX5-TDP-43 association on R-loops occurred in NIH3T3 cells as well as in mESC-differentiated cells when *Lnc530* was ectopically expressed. It seemed that the interaction did not require other mESC-specific factors and might be autonomous. Thus, we identified an lncRNA that can localize on R-loops to regulate R-loop homeostasis. To our knowledge, this is the first work to report the R-loop-resided regulatory lncRNA. In the future, systemic identification of R-loop-associated lncRNAs by utilizing synthetic DNA-RNA hybrids would provide more insights into the regulation of R-loop homeostasis.

How *Lnc530* stimulates the assembly of *Lnc530*-DDX5-TDP-43 complex to increase the local concentrations of DDX5 and TDP-43 is currently unknown. However, RNA-dependent condensate formation via phase separation could be an intriguing hypothesis. RNA and interacting

(C) Dot-blot analysis on genomic DNA confirmed that KD of TDP-43 or DDX5 increased R-loop levels in mESCs. Re-expression of TDP-43 or DDX5, or RNase H1 OE in KD cells rescued the defect.
(D) Quantification of dot-blot intensity in (C), with dsDNA as internal reference.
(E) CIdU incorporation assay showed that KD of TDP-43 or DDX5 increased the level of ssDNA monitored by CIdU (red). Re-expression of TDP-43 or DDX5, or RNase H1 OE in KD cells rescued the defect. Scale bars, 20 μm.
(F) Quantification of immunostaining intensity in (E). At least 20 visual fields containing 1,000 cells were analyzed in each group.
(G) Neutral comet assay revealed that KD of TDP-43 or DDX5 increased DNA DSBs level. Re-expression of TDP-43 or DDX5, or RNase H1 OE in KD cells rescued the defect. Left panel shows the quantification of comet tail length. Right panel shows representative images. At least 200 tails were analyzed in each group. Scale bar, 400 μm.
(H) More DDX5 KD and TDP-43 KD mESCs contained micronuclei. Left panel shows quantification result. Right panel shows the representative image of micronucleus (arrow). At least 50 visual fields containing 1,000 cells were analyzed in each group. Scale bars, 10 μm.
(I) DDX5 KD and TDP-43 KD mESCs displayed higher rate of aneuploidy. Left panel shows quantification result. Right panel shows representative images. At least 150 metaphase spreads were examined in three replications in each group. Scale bars, 20 μm.
All experiments were independently repeated three times with similar results. Data are shown as mean ± SD, two-tailed Student's t test.

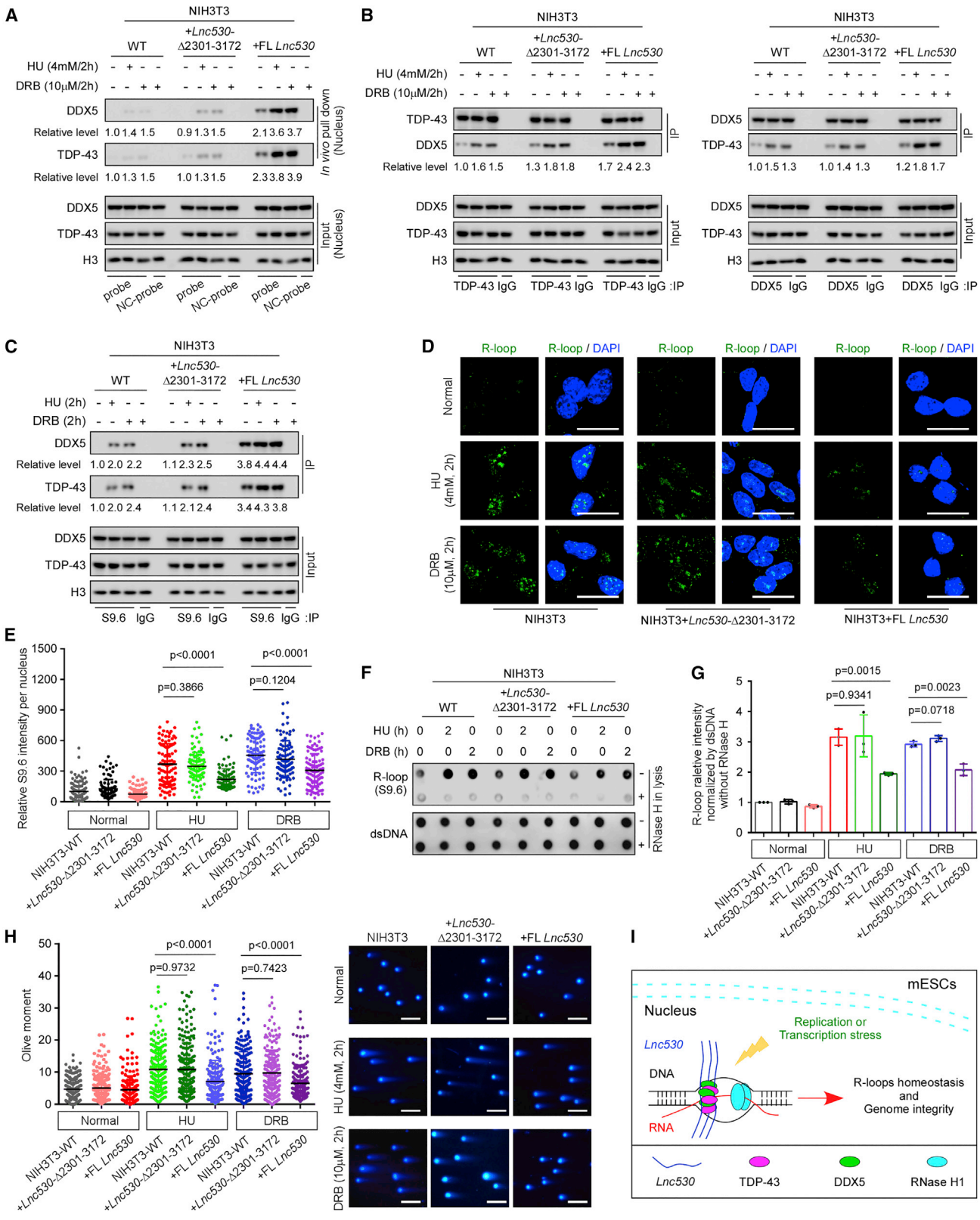

(legend on next page)

RNA-binding proteins can form condensates that specifically concentrate biomolecules to efficiently regulate key biological processes (Banani et al., 2017; Shin and Brangwynne, 2017). Both DDX5 and TDP-43 contain intrinsically disordered regions (IDRs) essential for induction of phase separation and formation of cellular condensates. Moreover, TDP-43 can undergo phase separation. In the future, whether *Lnc530*-DDX5-TDP-43 form condensates via phase separation warrants investigation.

Lnc530 interacted with TDP-43 and modulated its role. Dysfunction of TDP-43 was linked to neurodegenerative disorders, including ALS and frontotemporal dementia (FTD) (Hill et al., 2016; Mann et al., 2019; Neumann et al., 2006; Yin et al., 2012). Notably, we detected abundant expression of *Lnc530* in different brain regions of mice, with the levels higher than that in mESCs. These observations suggested that *Lnc530* could modulate the functions of TDP-43 in brain and therefore be involved in the pathogenesis of ALS and FTD. *Lnc530* is partially conserved between mouse and human. The functions of human *Lnc530* and its involvement in brain diseases warrant further study.

EXPERIMENTAL PROCEDURES

Resource availability

Corresponding author

Further information and requests for resources and reagents should be directed to the corresponding author, Ping Zheng (zhengp@mail.kiz.ac.cn).

Materials availability

All unique/stable reagents generated in this study are available from the corresponding author, Ping Zheng, with a completed Materials Transfer Agreement.

Data and code availability

All data needed to evaluate the conclusions in this paper are present in the paper and/or the supplemental information. The MS data for *in vivo* RNA pull-down have been deposited to the ProteomeXchange Consortium via the iProX repository with the dataset identifier PXD040075.

Cell lines and culture

MEFs were obtained from embryonic day 13.5 (E13.5) embryos of CD1 mice. MEFs, C2C12, and NIH3T3 cells were cultured in DMEM supplemented with 10% fetal bovine serum (Gibco, 10099141). WT mESCs were derived previously in our laboratory (Zhao et al., 2015) and cultured in DMEM/F12 medium supplemented with 20% Knockout serum replacement (Gibco, 10828028), 2 mM L-glutamine, 1 mM sodium pyruvate, 0.1 mM β-mercaptoethanol, 1% non-essential amino acids, and 1,000 units/mL mouse leukemia inhibitory factor (mLIF, Millipore, ESG1107).

qRT-PCR

Total RNA was extracted using Trizol (Tiangen, DP424), and 1.0 μg of total RNA was reverse transcribed using PrimeScript RT Reagent Kit (Takara, RR037A). qPCR was performed on CFX96 Real-Time System (Bio-Rad) using the TB Green Premix Ex Taq II Kit (Takara, RR820A). The primers for qPCR are listed in Table S2.

Lentivirus-mediated gene manipulation

The primers for gene cloning are listed in Table S3 and for gene knockdown by shRNAs in Table S4. All the shRNAs were constructed into pTRIPZ plasmid. FL and truncated *Lnc530* were amplified using overlap PCR and inserted into pEasy-Blunt plasmid (Transgene, CB101-01). pTOMO-EGFP-1×FLAG-TDP-43 was acquired from Prof. Baowei Jiao at the Kunming Institute of Zoology, Chinese Academy of Sciences. FLAG-tagged *Tdp-43-ΔRRM1* coding region (CDS) was amplified using overlap PCR and inserted into modified pTOMO-EGFP plasmid. *Rnase H1* and

Figure 7. Ectopic expression of *Lnc530* in NIH3T3 cells decreases R-loop formation and increases genome stability

(A) *In vivo* RNA pull-down assay confirmed that under HU or DRB treatment conditions, TDP-43 and DDX5 interacted with FL *Lnc530* but not *Lnc530* Δ2,301–3,172 ectopically expressed in NIH3T3 cells. NC-probe, negative control probe.

(B) Reciprocal IP showed that ectopic expression of FL *Lnc530*, but not *Lnc530* Δ2,301–3,172, increased TDP-43-DDX5 association in NIH3T3 cells. See also Figure S6.

(C) S9.6 IP showed that ectopic expression of FL *Lnc530*, but not *Lnc530* Δ2,301–3,172, increased the accumulation of TDP-43 and DDX5 on R-loops in NIH3T3 cells.

(D and E) Immunostaining (D) and quantification (E) revealed that OE of FL *Lnc530*, but not *Lnc530* Δ2,301–3,172, reduced the R-loop formation after HU or DRB treatment. At least 20 visual fields containing 500 cells were analyzed in three independent experiments. Scale bars, 20 μm.

(F and G) Dot-blot analysis (F) and quantification (G) confirmed that ectopic expression of FL *Lnc530*, but not *Lnc530* Δ2,301–3,172, decreased the R-loop formation after HU or DRB treatment. dsDNA was used as internal reference.

(H) Neutral comet assay showed that forced expression of FL *Lnc530*, but not *Lnc530* Δ2,301–3,172, alleviated DNA DSB formation after HU or DRB treatment. Left panel shows the quantification of comet tail length. Right panel shows representative images. At least 200 tails were analyzed in each group. Scale bar, 400 μm.

(I) Working model. LncRNA *Lnc530* recruited more TDP-43 and DDX5 proteins to R-loops to efficiently prevent undesirable R-loop formation. All experiments were independently repeated three times with similar results. The relative protein levels in (A)–(C) were normalized by input. Data are shown as mean ± SD, two-tailed Student's t test.

Ddx5 coding regions (CDS) were inserted into modified pTOMO-EGFP-3×FLAG plasmid. *Lnc530* ORF and *Floped* CDS containing FLAG tag were inserted into pcDNA3.1(+) plasmid. For expression of *Lnc530*, FL and truncated *Lnc530*-Δ2,301–3,172 were inserted into pCDH-CMV-GFP-Puro plasmid.

For the virus package, the plasmids were mixed with packaging plasmids psPAX2 and pMD2.G, and co-transfected into 293T cells. For gene knockdown and *Lnc530* expression, the puromycin (0.5 μg/mL) was added into culture medium for 48-h selection after lentivirus infection. For the pTOMO-mediated gene expression, GFP-positive cells were sorted by flow cytometry.

Immunofluorescent staining

Cells were fixed in 4% paraformaldehyde (PFA) for 10 min, followed by treatment with 0.2% Triton X-100, and blocked with 3% BSA at room temperature. The blocked cells were incubated with primary and secondary antibodies diluted in blocking solution, and the nuclei were counterstained with DAPI. Slides were sealed with glycerin. Images were captured using a confocal microscope (Olympus, FV1000).

For R-loop immunostaining, cells were first permeabilized with CSKT buffer (10 mM PIPES [pH = 6.8], 100 mM NaCl, 3 mM $MgCl_2$, 0.3 M sucrose, and 0.5% Triton X-100) at 4°C for 10 min. After that, procedures were carried out as in immunofluorescence staining.

RNA transcription assay was performed using EU-Click Kit (RiboBio, C10316-1). Cells were labeled with 500 μM 5-ethynyl uridine (EU) for 30 min, and immunostaining was carried out according to the manufacturer's protocol. Fluorescence intensity was measured by ImageJ (Version 1.52), and statistical analyses were performed using GraphPad Prism (Version 6.01). Antibody information was listed in Table S5.

Dot-blot analysis

Nucleic acids in nuclei were extracted by SDS/proteinase K buffer at 37°C overnight, followed by phenol-chloroform extraction and ethanol precipitation. DNA samples were treated with or without RNase H (New England Biolabs, M0297L), and blotted onto NC membrane. The membranes were air-dried, and blocked with 5% non-fat milk, followed by immunoblotting with primary and secondary antibodies. Images were collected from the Protein Simple FluorChem system (Protein Simple, FluorChem M FM0-561) and quantified using ImageJ (Version 1.52).

RNA-FISH

The probes and hybridization kit (C10910) were ordered from Guangzhou RiboBio. RNA-FISH was performed according to the manufacturer's protocol. Briefly, cells were permeabilized with CSKT buffer and fixed in 4% PFA. Hybridization was performed at 37°C overnight. Glass covers were washed three times with 4× saline sodium citrate buffer (SSC), once with 2× SSC, and once with 1× SSC at 42°C. Immunostaining was performed as described in section of immunofluorescent staining.

Immunoblotting

Total protein was extracted using RIPA buffer (Beyotime, P0013B) and subjected to SDS-PAGE gel separation. Proteins were then transferred to polyvinylidene fluoride (PVDF) membrane. Membranes were blocked and incubated with antibodies. Images were collected from the Protein Simple FluorChem system (Protein Simple, FluorChem M FM0-561) and quantified using ImageJ (Version 1.52). Antibody information is listed in Table S5.

IP

For IP analysis, cells were collected and lysed in RIPA buffer (Beyotime, P0013). The extracts were incubated with 2 μg of antibody or immunoglobulin G (IgG) and 30 μL of protein A/G-MagPoly beads (Abmart, A10002M) at 4°C overnight. Beads were washed and boiled with 2× SDS loading buffer for downstream immunoblotting analysis.

S9.6 IP

S9.6 IP analysis was performed as described previously (Cristini et al., 2018). Briefly, cells were re-suspended in RSB buffer (10 mM Tris-HCl [pH = 7.5], 200 mM NaCl, 2.5 mM $MgCl_2$, 0.5% Triton X-100) and sonicated for 10 min. The extracts were incubated with S9.6 antibody or IgG and beads, supplemented with 2 μL of RNase A (New England Biolabs, T3018L) at 4°C overnight. Beads were washed and eluted for downstream immunoblotting analysis. For detection of *Lnc530* on R-loops, the assay was performed as described previously (Gagliardi and Matarazzo, 2016).

In vivo RNA pull-down and MS analysis

The probes labeled with biotin at 3' end were ordered from Guangzhou RiboBio. *In vivo* RNA pull-down assay was performed as previously described (Chu et al., 2017). Briefly, cells were cross-linked with 265-nm UV light at 400 mJ of energy, and treated with CSKT buffer. After spinning, the pellet was re-suspended in DNase I buffer (50 mM Tris [pH = 7.5], 0.5% NP-40, 0.1% sodium lauroyl sarcosine, protease inhibitors, SUPERase-In, 600 U RNase free DNase I, 10 mM vanadyl ribonucleoside complex) and incubated at 37°C for 1 h. Supernatants were incubated with probes and M-280 streptavidin Dynabeads (Thermo, 00781251) at 65°C for 15 min. The proteins were eluted for downstream MS or immunoblotting analysis. Detailed methods for MS are available in the supplemental information.

Statistical analyses

Statistical analyses were performed by two-tailed Student's t test, two-way ANOVA with Bonferroni post using GraphPad Prism (Version 6.01). $p < 0.05$ was considered significant. All experiments were repeated three times using independent biological samples.

SUPPLEMENTAL INFORMATION

Supplemental information can be found online at https://doi.org/10.1016/j.stemcr.2023.02.003.

AUTHOR CONTRIBUTIONS

D.G. performed most of the experiments, analyzed the data, and prepared the figures. L.W. obtained the FL *Lnc530*. H.Z. and J.G. performed the MS analysis. W.Z. supervised the figure preparation. P.Z. supervised the study and wrote the manuscript.

ACKNOWLEDGMENTS

We thank Professor Baowei Jiao at Kunming Institute of Zoology, Chinese Academy of Sciences, for providing the pTOMO-IRES-EGFP-FLAG-TDP-43 plasmid, and Professor Hongjie Yao at Guangzhou Institute of Biomedicine and Health, Chinese Academy of Sciences, for providing S9.6 antibody. This work was supported by grants from the National Natural Science Foundation of China (31930027).

CONFLICT OF INTERESTS

The authors declare no competing interests.

Received: August 4, 2022
Revised: February 13, 2023
Accepted: February 13, 2023
Published: March 16, 2023

REFERENCES

Abakir, A., Giles, T.C., Cristini, A., Foster, J.M., Dai, N., Starczak, M., Rubio-Roldan, A., Li, M., Eleftheriou, M., Crutchley, J., et al. (2020). N(6)-methyladenosine regulates the stability of RNA:DNA hybrids in human cells. Nat. Genet. *52*, 48–55. https://doi.org/10.1038/s41588-019-0549-x.

Aguilera, A., and Garcia-Muse, T. (2012). R loops: from transcription byproducts to threats to genome stability. Mol. Cell *46*, 115–124. https://doi.org/10.1016/j.molcel.2012.04.009.

Aguilera, A., and Gómez-González, B. (2017). DNA-RNA hybrids: the risks of DNA breakage during transcription. Nat. Struct. Mol. Biol. *24*, 439–443. https://doi.org/10.1038/nsmb.3395.

Andrews, P.W., Barbaric, I., Benvenisty, N., Draper, J.S., Ludwig, T., Merkle, F.T., Sato, Y., Spits, C., Stacey, G.N., Wang, H., and Pera, M.F. (2022). The consequences of recurrent genetic and epigenetic variants in human pluripotent stem cells. Cell Stem Cell *29*, 1624–1636. https://doi.org/10.1016/j.stem.2022.11.006.

Armaos, A., Colantoni, A., Proietti, G., Rupert, J., and Tartaglia, G.G. (2021). catRAPID omics v2.0: going deeper and wider in the prediction of protein-RNA interactions. Nucleic Acids Res. *49*, W72–W79. https://doi.org/10.1093/nar/gkab393.

Arora, R., Lee, Y., Wischnewski, H., Brun, C.M., Schwarz, T., and Azzalin, C.M. (2014). RNaseH1 regulates TERRA-telomeric DNA hybrids and telomere maintenance in ALT tumour cells. Nat. Commun. *5*, 5220. https://doi.org/10.1038/ncomms6220.

Balk, B., Maicher, A., Dees, M., Klermund, J., Luke-Glaser, S., Bender, K., and Luke, B. (2013). Telomeric RNA-DNA hybrids affect telomere-length dynamics and senescence. Nat. Struct. Mol. Biol. *20*, 1199–1205. https://doi.org/10.1038/nsmb.2662.

Banani, S.F., Lee, H.O., Hyman, A.A., and Rosen, M.K. (2017). Biomolecular condensates: organizers of cellular biochemistry. Nat. Rev. Mol. Cell Biol. *18*, 285–298. https://doi.org/10.1038/nrm.2017.7.

Bhatia, V., Herrera-Moyano, E., Aguilera, A., and Gómez-González, B. (2017). The role of replication-associated repair factors on R-loops. Genes *8*, 171. https://doi.org/10.3390/genes8070171.

Björkman, A., Johansen, S.L., Lin, L., Schertzer, M., Kanellis, D.C., Katsori, A.M., Christensen, S.T., Luo, Y., Andersen, J.S., Elsässer, S.J., et al. (2020). Human RTEL1 associates with Poldip3 to facilitate responses to replication stress and R-loop resolution. Genes Dev. *34*, 1065–1074. https://doi.org/10.1101/gad.330050.119.

Boguslawski, S.J., Smith, D.E., Michalak, M.A., Mickelson, K.E., Yehle, C.O., Patterson, W.L., and Carrico, R.J. (1986). Characterization of monoclonal antibody to DNA.RNA and its application to immunodetection of hybrids. J. Immunol. Methods *89*, 123–130. https://doi.org/10.1016/0022-1759(86)90040-2.

Bou-Nader, C., Bothra, A., Garboczi, D.N., Leppla, S.H., and Zhang, J. (2022). Structural basis of R-loop recognition by the S9.6 monoclonal antibody. Nat. Commun. *13*, 1641. https://doi.org/10.1038/s41467-022-29187-7.

Buratti, E., and Baralle, F.E. (2001). Characterization and functional implications of the RNA binding properties of nuclear factor TDP-43, a novel splicing regulator of CFTR exon 9. J. Biol. Chem. *276*, 36337–36343. https://doi.org/10.1074/jbc.M104236200.

Castellano-Pozo, M., Santos-Pereira, J.M., Rondón, A.G., Barroso, S., Andújar, E., Pérez-Alegre, M., García-Muse, T., and Aguilera, A. (2013). R loops are linked to histone H3 S10 phosphorylation and chromatin condensation. Mol. Cell *52*, 583–590. https://doi.org/10.1016/j.molcel.2013.10.006.

Cerritelli, S.M., and Crouch, R.J. (2009). Ribonuclease H: the enzymes in eukaryotes. FEBS J. *276*, 1494–1505. https://doi.org/10.1111/j.1742-4658.2009.06908.x.

Cervantes, R.B., Stringer, J.R., Shao, C., Tischfield, J.A., and Stambrook, P.J. (2002). Embryonic stem cells and somatic cells differ in mutation frequency and type. Proc. Natl. Acad. Sci. USA *99*, 3586–3590. https://doi.org/10.1073/pnas.062527199.

Chu, H.P., Cifuentes-Rojas, C., Kesner, B., Aeby, E., Lee, H.G., Wei, C., Oh, H.J., Boukhali, M., Haas, W., and Lee, J.T. (2017). TERRA RNA antagonizes ATRX and protects telomeres. Cell *170*, 86–101.e16. https://doi.org/10.1016/j.cell.2017.06.017.

Costantino, L., and Koshland, D. (2015). The Yin and yang of R-loop biology. Curr. Opin. Cell Biol. *34*, 39–45. https://doi.org/10.1016/j.ceb.2015.04.008.

Cristini, A., Groh, M., Kristiansen, M.S., and Gromak, N. (2018). RNA/DNA hybrid interactome identifies DXH9 as a molecular player in transcriptional termination and R-loop-associated DNA damage. Cell Rep. *23*, 1891–1905. https://doi.org/10.1016/j.celrep.2018.04.025.

Cristini, A., Tellier, M., Constantinescu, F., Accalai, C., Albulescu, L.O., Heiringhoff, R., Bery, N., Sordet, O., Murphy, S., and Gromak, N. (2022). RNase H2, mutated in Aicardi-Goutieres syndrome, resolves co-transcriptional R-loops to prevent DNA breaks and inflammation. Nat. Commun. *13*, 2961. https://doi.org/10.1038/s41467-022-30604-0.

D'Ambrogio, A., Buratti, E., Stuani, C., Guarnaccia, C., Romano, M., Ayala, Y.M., and Baralle, F.E. (2009). Functional mapping of

the interaction between TDP-43 and hnRNP A2 in vivo. Nucleic Acids Res. *37*, 4116–4126. https://doi.org/10.1093/nar/gkp342.

Feretzaki, M., Pospisilova, M., Valador Fernandes, R., Lunardi, T., Krejci, L., and Lingner, J. (2020). RAD51-dependent recruitment of TERRA lncRNA to telomeres through R-loops. Nature *587*, 303–308. https://doi.org/10.1038/s41586-020-2815-6.

Frame, J.M., and North, T.E. (2021). Ddx41 loss R-loops in cGAS to fuel inflammatory HSPC production. Dev. Cell *56*, 571–572. https://doi.org/10.1016/j.devcel.2021.02.014.

Gagliardi, M., and Matarazzo, M.R. (2016). RIP: RNA immunoprecipitation. Methods Mol. Biol. *1480*, 73–86. https://doi.org/10.1007/978-1-4939-6380-5_7.

García-Muse, T., and Aguilera, A. (2019). R loops: from physiological to pathological roles. Cell *179*, 604–618. https://doi.org/10.1016/j.cell.2019.08.055.

Giannini, M., Bayona-Feliu, A., Sproviero, D., Barroso, S.I., Cereda, C., and Aguilera, A. (2020). TDP-43 mutations link Amyotrophic Lateral Sclerosis with R-loop homeostasis and R loop-mediated DNA damage. PLoS Genet. *16*, e1009260. https://doi.org/10.1371/journal.pgen.1009260.

Grunseich, C., Wang, I.X., Watts, J.A., Burdick, J.T., Guber, R.D., Zhu, Z., Bruzel, A., Lanman, T., Chen, K., Schindler, A.B., et al. (2018). Senataxin mutation reveals how R-loops promote transcription by blocking DNA methylation at gene promoters. Mol. Cell *69*, 426–437.e7. https://doi.org/10.1016/j.molcel.2017.12.030.

Hamperl, S., Bocek, M.J., Saldivar, J.C., Swigut, T., and Cimprich, K.A. (2017). Transcription-replication conflict orientation modulates R-loop levels and activates distinct DNA damage responses. Cell *170*, 774–786.e19. https://doi.org/10.1016/j.cell.2017.07.043.

Hamperl, S., and Cimprich, K.A. (2016). Conflict resolution in the genome: how transcription and replication make it work. Cell *167*, 1455–1467. https://doi.org/10.1016/j.cell.2016.09.053.

Hill, S.J., Mordes, D.A., Cameron, L.A., Neuberg, D.S., Landini, S., Eggan, K., and Livingston, D.M. (2016). Two familial ALS proteins function in prevention/repair of transcription-associated DNA damage. Proc. Natl. Acad. Sci. USA *113*, E7701–E7709. https://doi.org/10.1073/pnas.1611673113.

Kim, S., Kang, N., Park, S.H., Wells, J., Hwang, T., Ryu, E., Kim, B.G., Hwang, S., Kim, S.J., Kang, S., et al. (2020). ATAD5 restricts R-loop formation through PCNA unloading and RNA helicase maintenance at the replication fork. Nucleic Acids Res. *48*, 7218–7238. https://doi.org/10.1093/nar/gkaa501.

Kimbrel, E.A., and Lanza, R. (2015). Current status of pluripotent stem cells: moving the first therapies to the clinic. Nat. Rev. Drug Discov. *14*, 681–692. https://doi.org/10.1038/nrd4738.

Le, R., Huang, Y., Zhang, Y., Wang, H., Lin, J., Dong, Y., Li, Z., Guo, M., Kou, X., Zhao, Y., et al. (2021). Dcaf11 activates Zscan4-mediated alternative telomere lengthening in early embryos and embryonic stem cells. Cell Stem Cell *28*, 732–747.e9. https://doi.org/10.1016/j.stem.2020.11.018.

Li, X., and Manley, J.L. (2005). Inactivation of the SR protein splicing factor ASF/SF2 results in genomic instability. Cell *122*, 365–378. https://doi.org/10.1016/j.cell.2005.06.008.

Luo, H., Zhu, G., Eshelman, M.A., Fung, T.K., Lai, Q., Wang, F., Zeisig, B.B., Lesperance, J., Ma, X., Chen, S., et al. (2022). HOTTIP-dependent R-loop formation regulates CTCF boundary activity and TAD integrity in leukemia. Mol. Cell *82*, 833–851.e11. https://doi.org/10.1016/j.molcel.2022.01.014.

Mann, J.R., Gleixner, A.M., Mauna, J.C., Gomes, E., DeChellis-Marks, M.R., Needham, P.G., Copley, K.E., Hurtle, B., Portz, B., Pyles, N.J., et al. (2019). RNA binding antagonizes neurotoxic phase transitions of TDP-43. Neuron *102*, 321–338.e8. https://doi.org/10.1016/j.neuron.2019.01.048.

Maynard, S., Swistowska, A.M., Lee, J.W., Liu, Y., Liu, S.T., Da Cruz, A.B., Rao, M., de Souza-Pinto, N.C., Zeng, X., and Bohr, V.A. (2008). Human embryonic stem cells have enhanced repair of multiple forms of DNA damage. Stem Cell. *26*, 2266–2274. https://doi.org/10.1634/stemcells.2007-1041.

Mersaoui, S.Y., Yu, Z., Coulombe, Y., Karam, M., Busatto, F.F., Masson, J.Y., and Richard, S. (2019). Arginine methylation of the DDX5 helicase RGG/RG motif by PRMT5 regulates resolution of RNA:DNA hybrids. EMBO J. *38*, e100986. https://doi.org/10.15252/embj.2018100986.

Neumann, M., Sampathu, D.M., Kwong, L.K., Truax, A.C., Micsenyi, M.C., Chou, T.T., Bruce, J., Schuck, T., Grossman, M., Clark, C.M., et al. (2006). Ubiquitinated TDP-43 in frontotemporal lobar degeneration and amyotrophic lateral sclerosis. Science *314*, 130–133. https://doi.org/10.1126/science.1134108.

Ohle, C., Tesorero, R., Schermann, G., Dobrev, N., Sinning, I., and Fischer, T. (2016). Transient RNA-DNA hybrids are required for efficient double-strand break repair. Cell *167*, 1001–1013.e7. https://doi.org/10.1016/j.cell.2016.10.001.

Pappa, S., Padilla, N., Iacobucci, S., Vicioso, M., Álvarez de la Campa, E., Navarro, C., Marcos, E., de la Cruz, X., and Martínez-Balbás, M.A. (2019). PHF2 histone demethylase prevents DNA damage and genome instability by controlling cell cycle progression of neural progenitors. Proc. Natl. Acad. Sci. USA *116*, 19464–19473. https://doi.org/10.1073/pnas.1903188116.

Ribeiro, D.M., Zanzoni, A., Cipriano, A., Delli Ponti, R., Spinelli, L., Ballarino, M., Bozzoni, I., Tartaglia, G.G., and Brun, C. (2018). Protein complex scaffolding predicted as a prevalent function of long non-coding RNAs. Nucleic Acids Res. *46*, 917–928. https://doi.org/10.1093/nar/gkx1169.

Sankar, T.S., Wastuwidyaningtyas, B.D., Dong, Y., Lewis, S.A., and Wang, J.D. (2016). The nature of mutations induced by replication-transcription collisions. Nature *535*, 178–181. https://doi.org/10.1038/nature18316.

Sanz, L.A., Hartono, S.R., Lim, Y.W., Steyaert, S., Rajpurkar, A., Ginno, P.A., Xu, X., and Chédin, F. (2016). Prevalent, dynamic, and conserved R-loop structures associate with specific epigenomic signatures in mammals. Mol. Cell *63*, 167–178. https://doi.org/10.1016/j.molcel.2016.05.032.

Scalera, C., Ticli, G., Dutto, I., Cazzalini, O., Stivala, L.A., and Prosperi, E. (2021). Transcriptional stress induces chromatin relocation of the nucleotide excision repair factor XPG. Int. J. Mol. Sci. *22*, 6589. https://doi.org/10.3390/ijms22126589.

Shin, Y., and Brangwynne, C.P. (2017). Liquid phase condensation in cell physiology and disease. Science *357*, eaaf4382. https://doi.org/10.1126/science.aaf4382.

Skourti-Stathaki, K., Kamieniarz-Gdula, K., and Proudfoot, N.J. (2014). R-loops induce repressive chromatin marks over mammalian gene terminators. Nature *516*, 436–439. https://doi.org/10.1038/nature13787.

Skourti-Stathaki, K., and Proudfoot, N.J. (2014). A double-edged sword: R loops as threats to genome integrity and powerful regulators of gene expression. Genes Dev. *28*, 1384–1396. https://doi.org/10.1101/gad.242990.114.

Sollier, J., Stork, C.T., García-Rubio, M.L., Paulsen, R.D., Aguilera, A., and Cimprich, K.A. (2014). Transcription-coupled nucleotide excision repair factors promote R-loop-induced genome instability. Mol. Cell *56*, 777–785. https://doi.org/10.1016/j.molcel.2014.10.020.

Stolz, R., Sulthana, S., Hartono, S.R., Malig, M., Benham, C.J., and Chedin, F. (2019). Interplay between DNA sequence and negative superhelicity drives R-loop structures. Proc. Natl. Acad. Sci. USA *116*, 6260–6269. https://doi.org/10.1073/pnas.1819476116.

Takahashi, K., and Yamanaka, S. (2016). A decade of transcription factor-mediated reprogramming to pluripotency. Nat. Rev. Mol. Cell Biol. *17*, 183–193. https://doi.org/10.1038/nrm.2016.8.

Tichy, E.D., and Stambrook, P.J. (2008). DNA repair in murine embryonic stem cells and differentiated cells. Exp. Cell Res. *314*, 1929–1936. https://doi.org/10.1016/j.yexcr.2008.02.007.

Vohhodina, J., Goehring, L.J., Liu, B., Kong, Q., Botchkarev, V.V., Jr., Huynh, M., Liu, Z., Abderazzaq, F.O., Clark, A.P., Ficarro, S.B., et al. (2021). BRCA1 binds TERRA RNA and suppresses R-Loop-based telomeric DNA damage. Nat. Commun. *12*, 3542. https://doi.org/10.1038/s41467-021-23716-6.

Walker, C., Herranz-Martin, S., Karyka, E., Liao, C., Lewis, K., Elsayed, W., Lukashchuk, V., Chiang, S.C., Ray, S., Mulcahy, P.J., et al. (2017). C9orf72 expansion disrupts ATM-mediated chromosomal break repair. Nat. Neurosci. *20*, 1225–1235. https://doi.org/10.1038/nn.4604.

Wang, I.X., Grunseich, C., Fox, J., Burdick, J., Zhu, Z., Ravazian, N., Hafner, M., and Cheung, V.G. (2018). Human proteins that interact with RNA/DNA hybrids. Genome Res. *28*, 1405–1414. https://doi.org/10.1101/gr.237362.118.

Wang, L., Li, J., Zhou, H., Zhang, W., Gao, J., and Zheng, P. (2021). A novel lncRNA Discn fine-tunes replication protein A (RPA) availability to promote genomic stability. Nat. Commun. *12*, 5572. https://doi.org/10.1038/s41467-021-25827-6.

Wood, M., Quinet, A., Lin, Y.L., Davis, A.A., Pasero, P., Ayala, Y.M., and Vindigni, A. (2020). TDP-43 dysfunction results in R-loop accumulation and DNA replication defects. J. Cell Sci. *133*, jcs244129. https://doi.org/10.1242/jcs.244129.

Xiong, J., Todorova, D., Su, N.Y., Kim, J., Lee, P.J., Shen, Z., Briggs, S.P., and Xu, Y. (2015). Stemness factor Sall4 is required for DNA damage response in embryonic stem cells. J. Cell Biol. *208*, 513–520. https://doi.org/10.1083/jcb.201408106.

Yan, Q., Wulfridge, P., Doherty, J., Fernandez-Luna, J.L., Real, P.J., Tang, H.Y., and Sarma, K. (2022). Proximity labeling identifies a repertoire of site-specific R-loop modulators. Nat. Commun. *13*, 53. https://doi.org/10.1038/s41467-021-27722-6.

Yasuhara, T., Kato, R., Hagiwara, Y., Shiotani, B., Yamauchi, M., Nakada, S., Shibata, A., and Miyagawa, K. (2018). Human Rad52 promotes XPG-mediated R-loop processing to initiate transcription-associated homologous recombination repair. Cell *175*, 558–570.e11. https://doi.org/10.1016/j.cell.2018.08.056.

Yin, H.Z., Nalbandian, A., Hsu, C.I., Li, S., Llewellyn, K.J., Mozaffar, T., Kimonis, V.E., and Weiss, J.H. (2012). Slow development of ALS-like spinal cord pathology in mutant valosin-containing protein gene knock-in mice. Cell Death Dis. *3*, e374. https://doi.org/10.1038/cddis.2012.115.

Zhang, W., Chen, Z., Zhang, D., Zhao, B., Liu, L., Xie, Z., Yao, Y., and Zheng, P. (2019). KHDC3L mutation causes recurrent pregnancy loss by inducing genomic instability of human early embryonic cells. PLoS Biol. *17*, e3000468. https://doi.org/10.1371/journal.pbio.3000468.

Zhao, B., Zhang, W., Cun, Y., Li, J., Liu, Y., Gao, J., Zhu, H., Zhou, H., Zhang, R., and Zheng, P. (2018). Mouse embryonic stem cells have increased capacity for replication fork restart driven by the specific Filia-Floped protein complex. Cell Res. *28*, 69–89. https://doi.org/10.1038/cr.2017.139.

Zhao, B., Zhang, W.D., Duan, Y.L., Lu, Y.Q., Cun, Y.X., Li, C.H., Guo, K., Nie, W.H., Li, L., Zhang, R., and Zheng, P. (2015). Filia is an ESC-specific regulator of DNA damage response and safeguards genomic stability. Cell Stem Cell *16*, 684–698. https://doi.org/10.1016/j.stem.2015.03.017.

Stem Cell Reports, Volume *18*

Supplemental Information

Long noncoding RNA *Lnc530* localizes on R-loops and regulates R-loop formation and genomic stability in mouse embryonic stem cells

Daohua Gong, Lin Wang, Hu Zhou, Jing Gao, Weidao Zhang, and Ping Zheng

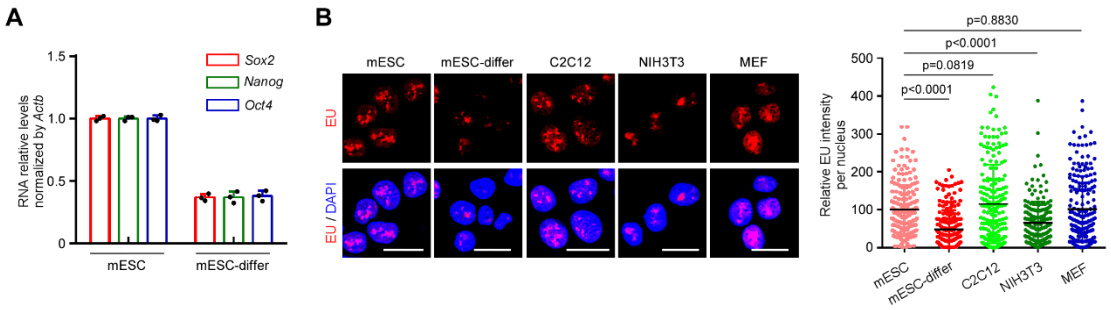

Figure S1. Evaluation of nascent RNA synthesis in mESCs and differentiated cells, related to Figure 1.

(**A**) Quantitative RT-PCR showed the relative mRNA expression of core pluripotency regulators *Sox2*, *Nanog* and *Oct4* in mESCs and mESC-differentiated (mESC-differ) cells. *Actb* was set as internal reference.

(**B**) Nascent RNA was monitored by EU (red). Immunostaining detected the RNA transcription in mESCs and differentiated cells. Left panel showed the representative immunostaining images. Right panel showed the quantification of EU intensity per nucleus. Scale bar, 20 μm.

All experiments were independently repeated three times with similar results. Data were shown as mean ± SD, two-tailed Student's *t*-test.

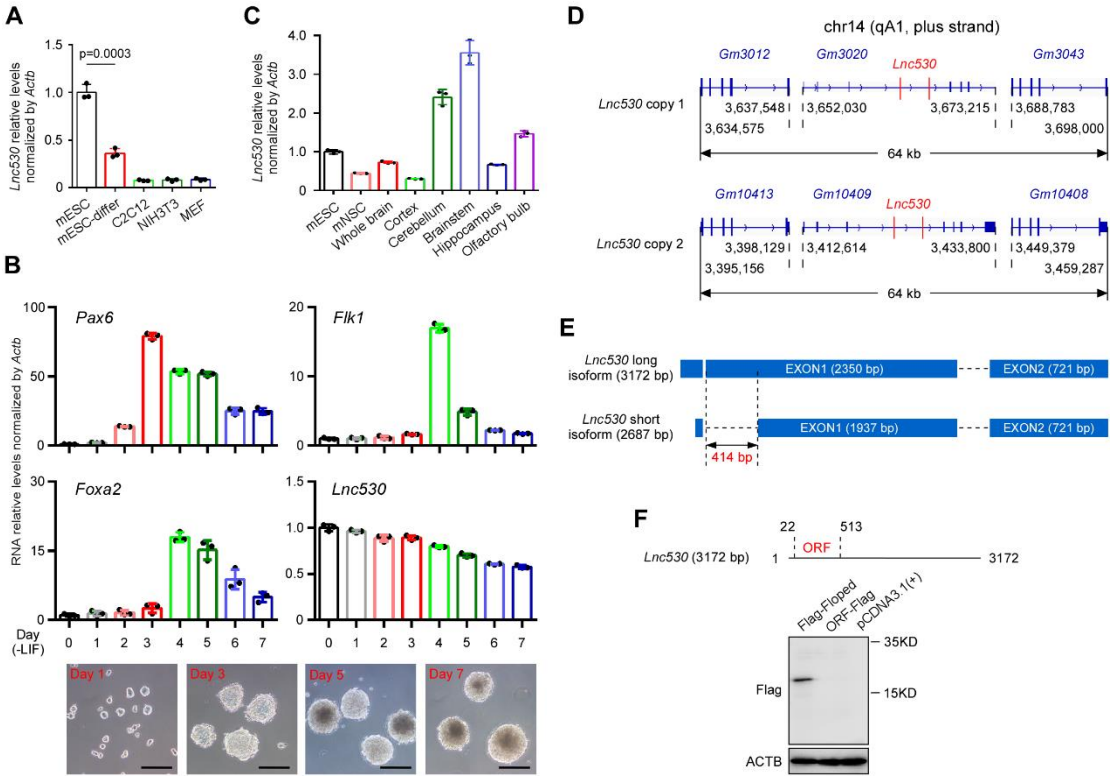

Figure S2. Characterization of *Lnc530* in mESCs.

(**A**) Quantitative RT-PCR showed that *Lnc530* was expressed in mESCs compared to several differentiated cell types under normal culture condition. *Actb* was set as internal reference.

(**B**) Quantitative RT-PCR showed the relative expression levels of four genes (*Pax6*, *Flk1*, *Foxa2* and *Lnc530*) in embryoid bodies (EBs) differentiated from mESCs for different time points. Lower panel showed the representative images of EBs. *Pax6* is an ectodermal marker, *Flk*1 is a mesodermal marker, *Foxa2* is an endodermal marker. *Actb* was set as internal reference. Scale bar, 200 μm.

(**C**) Quantitative RT-PCR showed the relative expression levels of *Lnc530* in different encephalic regions of C57BL/6 mice. *Actb* was set as internal reference.

(**D**) Based on mouse reference genome assembly version mm10, *Lnc530* gene has two genomic copies and is located on plus strand of chromosome 14.

(**E**) Two isoforms of *Lnc530*.

(**F**) The potential coding region of *Lnc530* did not encode protein or peptide. The Flag-tagged Floped protein was used as a positive control and pcDNA3.1 (+) was a negative control.

All experiments were independently repeated three times with similar results. Data were shown as mean ± SD, two-tailed Student's *t*-test.

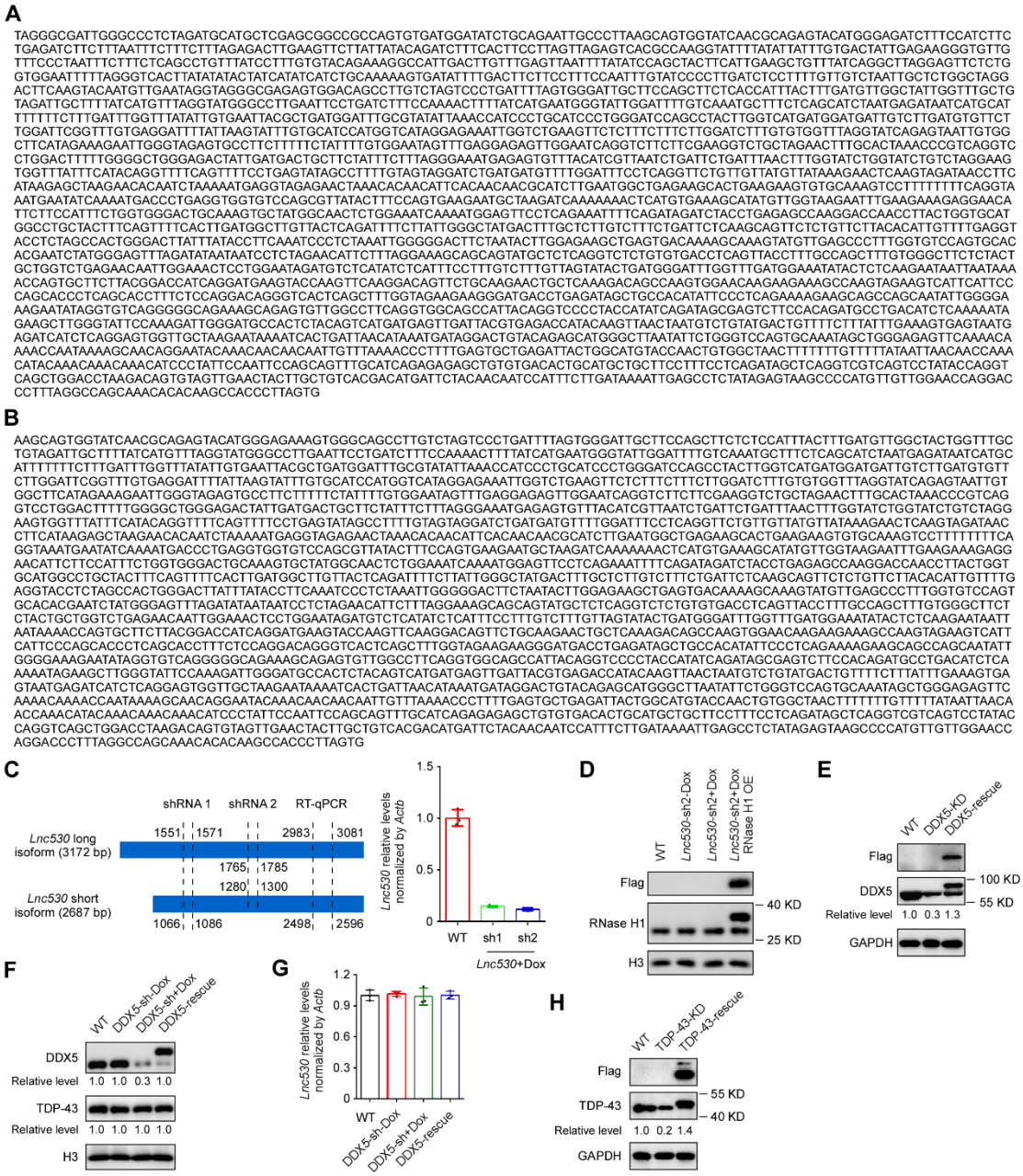

Figure S3. Establishment of gene Knockdown (KD) or over-expression mESCs, related to Figure 3 and 4.

(**A**) The sequence of *Lnc530* long isoform.

(**B**) The sequence of *Lnc530* short isoform.

(**C**) Quantitative RT-PCR confirmed the efficient KD of *Lnc530* in mESCs by two independent shRNAs. The shRNA targeting sites and qPCR primer targeting sites were indicated in left panel. *Actb* was set as internal reference.

(**D**) Immunoblotting confirmed the over-expression (OE) of RNase H1 in *Lnc530* KD mESCs.

(**E**) Immunoblotting verified the KD and re-expression of DDX5 (DDX5-rescue) in mESCs.

(**F**) Immunoblotting showed that KD or re-expression of DDX5 (DDX5-rescue) did not affect the expression of TDP-43 in mESCs.

(**G**) Quantitative RT-PCR showed the expression of *Lnc530* was not altered by DDX5 KD or

re-expression (DDX5-rescue). *Actb* was set as internal reference.

(**H**) Immunoblotting confirmed the KD and re-expression of TDP-43 (TDP-43-rescue) in mESCs.

All experiments were independently repeated three times with similar results. The relative protein levels in (E, F, H) were normalized by GAPDH or H3. Data were shown as mean ± SD, two-tailed Student's *t*-test.

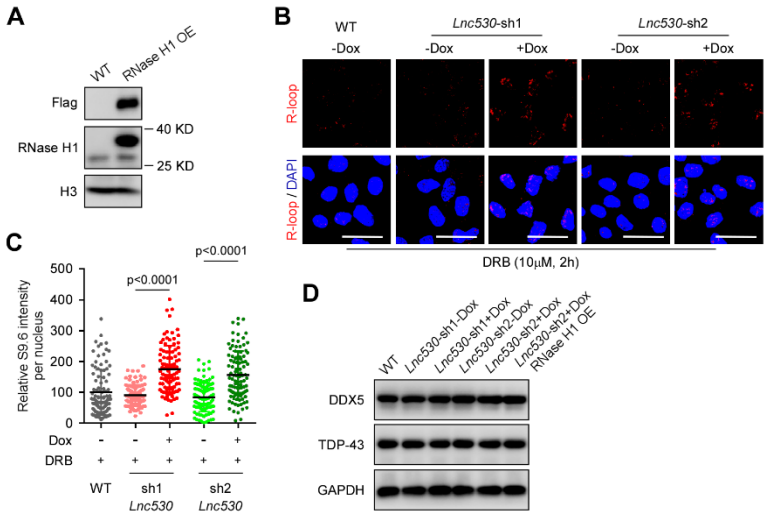

Figure S4. Loss of *Lnc530* perturbs R-loop homeostasis, related to Figure 5.

(**A**) Immunoblotting showed the over-expression (OE) of RNase H1 in wild-type mESCs.

(**B** and **C**) Immunostaining (B) and its quantification (C) revealed that *Lnc530* KD mESCs contained higher level of R-loops after DRB treatment. Scale bars, 30 μm. DNA was counterstained with DAPI. At least 20 visual fields containing 500 cells were analyzed in three independent experiments. Scale bars, 30 μm.

(**D**) Immunoblotting showed that the protein expressions of TDP-43 and DDX5 were not altered by *Lnc530* KD or/and RNase H1 over-expression (OE) in mESCs.

All experiments were independently repeated three times with similar results. Data were shown as mean ± SD, two-tailed Student's *t*-test.

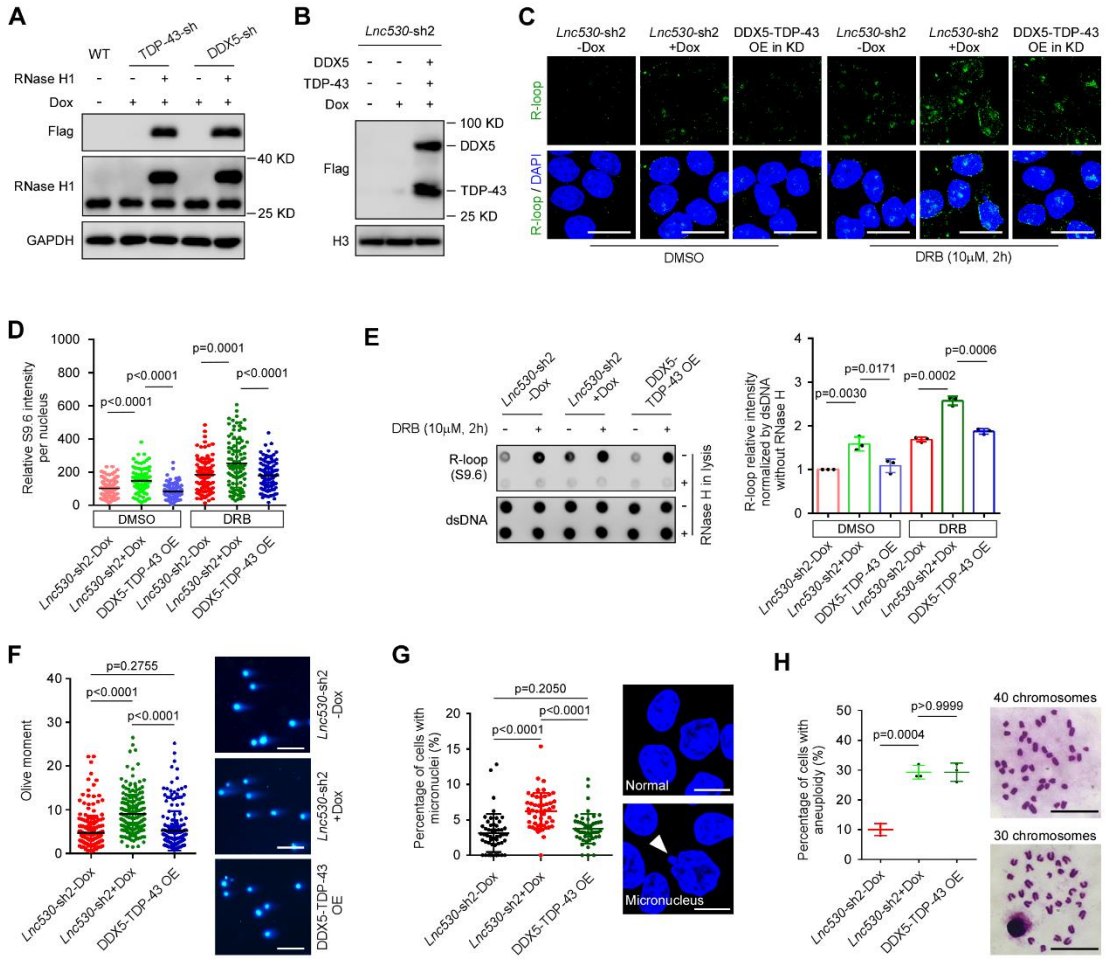

Figure S5. Over-expression of TDP-43 and DDX5 in *Lnc530* KD mESCs reduces the aberrant R-loop formation and DNA DSBs.

(**A**) Immunoblotting confirmed the forced expression of RNase H1 in TDP-43 KD or DDX5 KD mESCs.

(**B**) Immunoblotting verified the over-expression of DDX5 and TDP-43 proteins in *Lnc530* KD mESCs.

(**C** and **D**) Immunostaining showed that TDP-43 and DDX5 over-expression (OE) in *Lnc530* KD mESCs reduced R-loop formation (C). The quantification of R-loops per nucleus was shown in (D). At least 20 visual fields containing 500 cells were analyzed in three independent replications. Scale bar, 20 μm.

(**E**) Dot blot analysis of R-loops in *Lnc530*-KD mESCs with TDP-43 and DDX5 over-expression (OE). Left panel showed the dot blot images. Right panel was the quantification of dot blot intensity. dsDNA was set as internal reference.

(**F**) Neutral comet assay showed that TDP-43 and DDX5 over-expression (OE) in *Lnc530* KD mESCs reduced the generation of DNA DSBs. Left panel was the quantification of comet tail length. Right panel showed the representative images. At least 200 tails were analyzed in each group. Scale bars, 400 μm.

(**G**) Immunostaining showed that TDP-43 and DDX5 over-expression (OE) in *Lnc530* KD mESCs reduced the micronuclei formation. Left panel was the quantification. Right panel showed the representative images of micronucleus (arrow). At least 50 visual fields containing

1000 cells were analyzed in each group. Scale bars, 10 μm.

(**H**) TDP-43 and DDX5 over-expression (OE) in *Lnc530* KD mESCs failed to reduce the aneuploidy rate. Left panel was the quantification. Right panel showed the representative images. At least 150 metaphase spreads were examined in three replications in each group. Scale bars, 20 μm.

All experiments were repeated three times with similar results. Data were shown as mean ± SD, two-tailed Student's *t*-test.

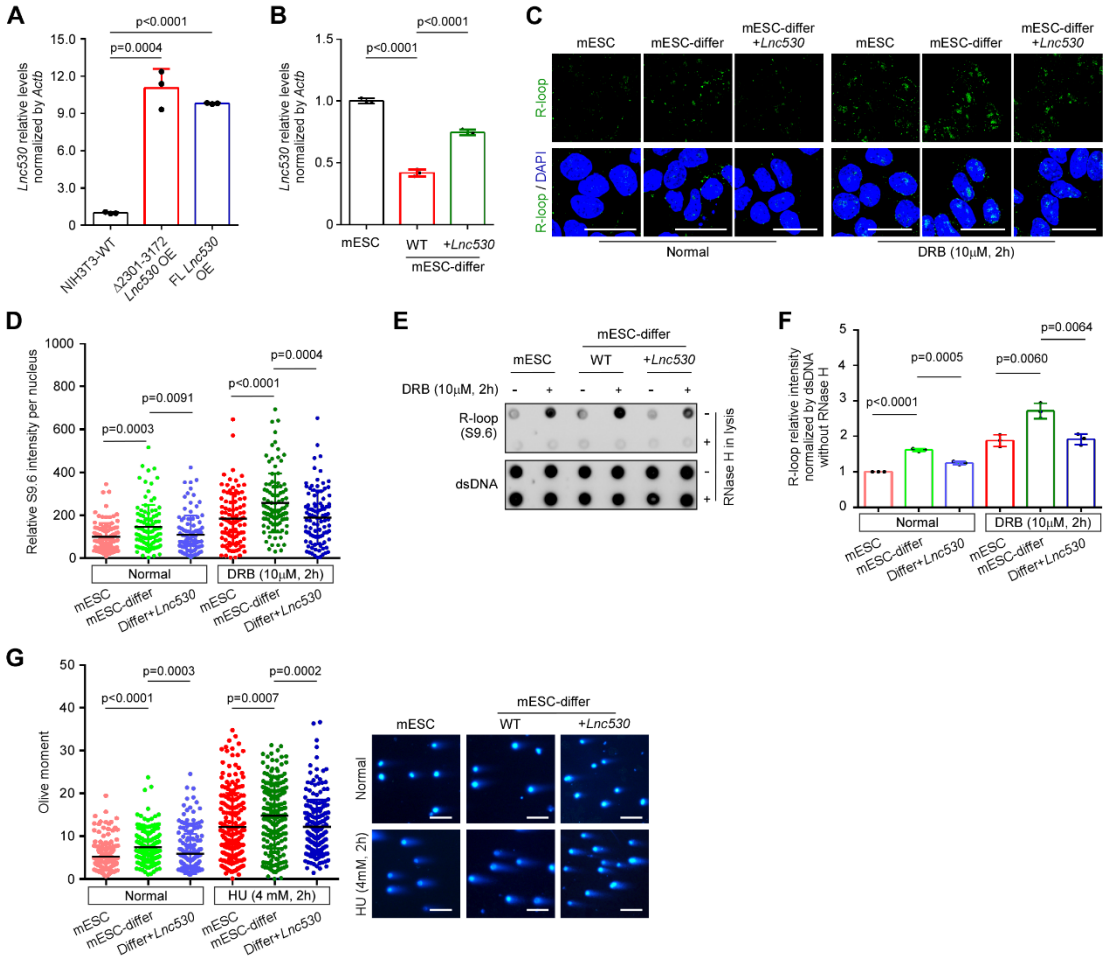

Figure S6. Over-expression of *Lnc530* in mESC-differentiated cells reduces R-loop formation and DNA damage.

(**A**) Quantitative RT-PCR confirmed the over-expression (OE) of full length (FL) *Lnc530* and Δ2301-3172 *Lnc530* in NIH3T3 cells. *Actb* was set as internal reference.

(**B**) The relative expression levels of *Lnc530* in mESCs, isogenic differentiated cells, and isogenic differentiated cells with *Lnc530* over-expression. *Actb* was set as internal reference.

(**C** and **D**) Immunostaining showed that over-expression of *Lnc530* in mESC-differentiated cells (mESC-differ) decreased the R-loop formation (C). The quantification of R-loops was shown in (D). At least 20 visual fields containing 500 cells were analyzed in three independent replications in each group. Scale bar, 20 μm.

(**E** and **F**) Dot blot analysis of R-loops in mESCs, mESC-differentiated cells (mESC-differ), and differentiated cells over-expressing *Lnc530* (E). The quantification of dot blot intensity was shown in (F). dsDNA was used as internal reference.

(**G**) Neutral comet assay revealed that over-expression of *Lnc530* in mESC-differentiated cells reduced the level of DNA DSBs. Left panel was the quantification of comet tail length. Right panel showed the representative images. At least 200 tails were analyzed in each group. Scale bars, 400 μm.

All experiments were repeated three times with similar results. Data were shown as mean ± SD, two-tailed Student's *t*-test.

Table S1. Protein candidates interacting with *Lnc530*.

Protein	Unique peptide counts					
	Negative control		Normal culture		4mM HU treatment	
	replicate 1	replicate 2	replicate 1	replicate 2	replicate 1	replicate 2
DDX5	0	0	0	1	2	3
TDP-43	0	0	0	0	1	2
Rplp0	0	0	0	0	2	1
Rpl3	0	0	0	0	2	2
Rpl4	0	0	0	0	5	5
Rpl7a	0	0	0	0	1	3
Rpl9	0	0	0	0	1	1
Rpl18	0	0	0	0	2	1
Rpl19	0	0	0	0	2	2
Rpl26	0	0	0	0	1	2
Rpl28	0	0	0	0	1	1
Rpl29	0	0	0	0	1	1
Hist1h1d	0	0	0	0	1	1
Rps8	0	0	0	0	1	3
Rps4x	0	0	0	0	2	2
GAPDH	0	0	0	0	1	1
Jup	0	0	0	0	3	1
Ctnnbl1	0	0	0	0	1	1

Table S2. Primers for RT-qPCR.

Gene	RT-PCR primers	
Lnc530	Forward	5’-TCAGATAGCTCAGGTCGTCAGT-3’
	Reverse	5’-AAGGATTGTTGTAGAATCATGTCG-3’
Actb	Forward	5’-TTGCTGATCCACATCTGCTGGAAGG-3’
	Reverse	5’-GTGTGACGTTGACATCCGTAAAGAC-3’
Sox2	Forward	5’-GACCGGCGGCAACCAGAAG-3’
	Reverse	5’-GCGCTTGCTGATCTCCGAGT-3’
Nanog	Forward	5’-AAAGGATGAAGTGCAAGCGGTG-3’
	Reverse	5’-TTCCAGATGCGTTCACCAGATA-3’
Oct4	Forward	5’-AGGAGCTAGAACAGTTTGCCAA-3’
	Reverse	5’-TTCTCATTGTTGTCGGCTTCCT-3’
Pax6	Forward	5’-TACCAGTGTCTACCAGCCAAT-3’
	Reverse	5’-TGCACGAGTATGAGGAGGTCT-3’
Flk1	Forward	5’-TTTGGCAAATACAACCCTTCAGA-3’
	Reverse	5’-GCAGAAGATACTGTCACCACC-3’
Foxa2	Forward	5’-CCCTACGCCAACATGAACTCG-3’
	Reverse	5’-GTTCTGCCGGTAGAAAGGGA-3’

Table S3. Primers for PCR cloning.

Gene	RACE and ORF or CDS primers	
Lnc530 RACE	GSP1	5'-AAACCGAATCCAAGAACACATC-3'
	GSP2	5'-GGTCGTCAGTCCTATACCAGGT-3'
Lnc530-full length (pCDH-CMV)	Forward	5'-TGACCTCCATAGAAGATTCTAGATAGGGCGATTGGGCCCTCTAGAT-3'
	Reverse	5'-AGATCCTTCGCGGCCGCGGATCCCACTAAGGGTGGCTTGTGTGT-3'
Lnc530-∆2301-3172 (pCDH-CMV)	Forward	5'-TGACCTCCATAGAAGATTCTAGATAGGGCGATTGGGCCCTCTAGAT-3'
	Reverse	5'-AGATCCTTCGCGGCCGCGGATCCGGGAATGAATGACTTCTACTTG-3'
Lnc530-ORF	Forward	5'-GAATTCATGCATGCTCGAGCGGCCGCCA-3'
	Reverse	5'-GAATTCCTACTTATCGTCGTCATCCTTGTAATCCCTATTCAACATTGTACTTGAAGT-3'
∆2301-3172 (pEasy-Blunt)	Forward	5'-TAGGGCGATTGGGCCCTCTAGATGCA-3'
	Reverse	5'-GGGAATGAATGACTTCTACTTGGCT-3'
∆1-2300 (pEasy-Blunt)	Forward	5'-AGCACCCTCAGCACCTTTCTCCAGGA-3'
	Reverse	5'-CACTAAGGGTGGCTTGTGTGTTTGC-3'
∆2601-3172 (pEasy-Blunt)	Forward	5'-TAGGGCGATTGGGCCCTCTAGATGCA-3'
	Reverse	5'-GGTCTCACGTAATCAACTCATCATGA-3'
∆2301-2600 (pEasy-Blunt)	Forward-1	5'-TAGGGCGATTGGGCCCTCTAGATGCA-3'
	Reverse-1	5'-CATACAGACATTAGTTAACTTGTATGGGAATGAATGACTTCTACTTGGCT-3'
	Forward-2	5'-AGCCAAGTAGAAGTCATTCATTCCCATACAAGTTAACTAATGTCTGTATG-3'
	Reverse-2	5'-CACTAAGGGTGGCTTGTGTGTTTGC-3'
Tdp-43-∆*RRM1*	Forward-1	5'-TCTAGAGCCACCATGGACTACAAGGACGACGATGACAAGATGTCTGAATATATTCGG-3
	Reverse-1	5'-TGGGCTTTGCTTAGAGTTGGGAAGGAGGTCAGATGTTTTCTGGACT-3
	Forward-2	5'-AGTCCAGAAAACATCTGACCTCCTTCCCAACTCTAAGCAAAGCCCA-3
	Reverse-2	5'-CGCGGATCCCTACATTCCCCAGCCAGAAG-3
Ddx5-CDS	Forward	5'-CTAGCTAGCTCGAGTTATTCTAGTGACCGAGA-3'
	Reverse	5'-CGCGGATCCTTATTGAGAATACCCTGTTGGCAT-3'
Rnase H1-CDS	Forward	5'-CTAGCTAGCTTCTATGCGGTGAGGAGAGGCCG-3'
	Reverse	5'-CGCGGATCCTCAGTCCTCAGACTGCTTCGCT-3'

Table S4. Short hairpin RNA sequences used for gene knockdown.

Gene	shRNA mir
Lnc530-shRNA1	5’-TGCTGTTGACAGTGAGCGCGGTGAGAATTTGAAGAAAGAGTA GTGAAGCCACAGATGTACTCTTTCTTCAAATTCTCACCATGCCTA CTGCCTCGGA -3’
Lnc530-shRNA2	5’-TGCTGTTGACAGTGAGCGCCTTGTCTTTCTGATTCTCAAGTAG TGAAGCCACAGATGTACTTGAGAATCAGAAAGACAAGATGCCTAC TGCCTCGGA-3’
Tdp-43-shRNA	5’-TGCTGTTGACAGTGAGCGCTCGCTGTGTCTCATTATCTAGTAG TGAAGCCACAGATGTACTAGATAATGAGACACAGCGATTGCCTAC TGCCTCGGA-3’
Ddx5-shRNA	5’-TGCTGTTGACAGTGAGCGACCTGTGGTTGTCTTAACTAATTAG TGAAGCCACAGATGTAATTAGTTAAGACAACCACAGGCTGCCTAC TGCCTCGGA-3’

Table S5. Antibody and drug information.

Antibodies	Source	Dilution
DDX5 Rabbit monoclonal antibody	Abcam; Cat# ab126730	1:1000 (IF) 1:1000 (IB) 1:50 (IP)
TDP-43 Rabbit monoclonal antibody	Abcam; Cat# ab190963	1:200 (IF) 1:1000 (IB) 1:50 (IP)
S9.6 Mouse monoclonal antibody	Kerafast; Cat# ENH001	1:100 (IF)
S9.6 Mouse monoclonal antibody	ATCC; Cat# HB-8730	1:50 (IP) 1:500 (Dot blot)
dsDNA Mouse monoclonal antibody	Santa Crus Biotechnology; Cat# sc-58749	1:500 (Dot blot)
BrdU Rat monoclonal antibody, also used for immunostaining of CIdU	Abcam; Cat# ab6326	1:1000 (IF)
γH2AX Rabbit polyclonal antibody	Cell Signaling Technology; Cat# 9718	1:1000 (IB) 1:1000 (IF)
RNase H1 Mouse monoclonal antibody	Santa Crus Biotechnology; Cat# sc-376326	1:500 (IB)
GAPDH Mouse monoclonal antibody	Sangon Biotech; Cat# D190090	1:1000 (IB)
Flag Rabbit polyclonal antibody	Sigma; Cat# F7425	1:1000 (IB)
SOX2 Rabbit polyclonal antibody	Merck Millipore; Cat# AB5603	1:500 (IB)
NANOG Rabbit polyclonal antibody	Abcam; Cat# ab70482	1:1000 (IB)
OCT4 Rabbit polyclonal antibody	Abcam; Cat# ab19857	1:1000 (IB)
Fibrillarin Rabbit monoclonal antibody	Cell Signaling Technology; Cat# 2639	1:1000 (IF)
Histone H3 Mouse monoclonal antibody	TransGen Biotech; Cat# HL102	1:1000 (IB)
ACTB Mouse monoclonal antibody	Abclonal; Cat# AC004	1:1000 (IB)
Goat anti-Rat IgG secondary antibody, Alexa Fluor Cy3	Thermo Fisher Scientific; Cat# A-10522	1:500 (IF)
Goat anti-Mouse IgG (H+L) secondary antibody, Alexa Fluor 488	Thermo Fisher Scientific; Cat# A-11029	1:500 (IF)
Donkey anti-Mouse IgG (H+L) Secondary Antibody, Alexa Fluor 555	Thermo Fisher Scientific; Cat# A-31570	1:500 (IF)
Goat anti-Rabbit IgG (H+L) Secondary Antibody, Alexa Fluor 488	Thermo Fisher Scientific; Cat# A-11034	1:500 (IF)
Donkey anti-Rabbit IgG (H+L) Secondary Antibody, Alexa Fluor 555	Thermo Fisher Scientific; Cat# A-31572	1:500 (IF)
Goat anti-Mouse IgG (H+L)	Thermo Fisher Scientific;	1:5000 (IB)

secondary antibody, HRP	Cat# 31430	
Goat anti-Rabbit IgG (H+L) secondary antibody, HRP	Thermo Fisher Scientific; Cat# 31460	1:5000 (IB)
5-Chloro-2′-deoxyuridine (CIdU)	Sigma-Aldrich; Cat# C6891	20 μM
Hydroxylurea (HU)	Sigma-Aldrich; Cat# H8627	4 mM
5,6-Dichlorobenzimidazole 1-β-D-Ribofuranoside	Tokyo Chemical Industry; Cat# ; D4292	10 μM

Supplemental experimental procedures

Mouse ESC differentiation

Mouse embryoid bodies (EBs) formation and mESCs differentiation were performed as previously described (Fu et al., 2022). Briefly, mESCs were cultured in mESC medium without LIF in an ultra-low attachment dish for EBs formation. EBs were collected at the indicated time points. For regular differentiation, mESCs were cultured in mESCs medium without LIF for 14 days in culture dish pre-coated with gelatin.

Rapid amplification of cDNA ends (RACE)

The RACE protocol is based on published Smart-seq2 protocol (Picelli et al., 2014). The oligo-dT primer, template-switching oligos (TSO) and ISPCR primers were synthesized as described in the Smart-seq2 method. 5' end and 3' end of *Lnc530* were amplified using ISPCR primer and gene specific primer 1 (GSP1) or gene specific primer 2 (GSP2), respectively. The products were cloned into pEasy-Blunt plasmid (Transgene, CB101-01). The primers were listed in Table S3.

Neutral comet assay

The neutral comet assay was performed as previously described (Zhao et al., 2015). Briefly, cells were dissociated and mixed with low-melting agarose, and spread onto the slides. The cells on slides were lyzed in lysis buffer [2.5 M NaCl, 100 mM EDTA, 10 mM Tris (pH = 8.3), 1% N-lauroylsarcosine, and 1% Triton X-100] for 1 h. Electrophoresis was performed for 30 min in buffer [300 mM sodium acetate, 100 mM Tris (pH = 8.3)]. The slides were washed and fixed with 100% ethanol, followed by staining with DAPI. The comet tails were analyzed by Komet 7 comet assay software (Andor Technology).

Karyotyping

The cultured cells were treated with 120 ng/mL colcemid (Gibco, 15212-012) for 2 h, digested and re-suspended with hypotonic buffer (75 mM KCl) for 15 min at 37 °C. The hypotonic cells were fixed with methanol/glacial acetic acid (3:1), dropped onto glass slides, and air-dried. Samples were stained with 3% Giemsa buffer (Gibco, 10092013) at 37 °C for 30 min. Images were captured using a Leica TCS SP5 confocal microscope system (Leica Microsystems).

Cell proliferation assay

The cell proliferation assay was performed with Click-iT™ EdU Kit (Thermo, C10337). Briefly, cells were labeled with 20 μM EdU (5-ethynyl-2'-deoxyuridine) for 2 h, digested and suspended in 4% PFA for 30 min, followed by treatment with 0.2% Triton X-100 for 20 min. Cells were incubated with reaction buffer prepared according to the manufacturer's protocol and sorted by flow cytometry.

In vitro RNA pull down

RNA was *in vitro* transcribed with T7 RNA polymerase (Fermentas, EP0111), and labeled with biotin using Pierce™ RNA 3' End Desthiobiotinylation Kit (Thermo, 20163). *In vitro* RNA

pull down assay was performed as previously described (Wang et al., 2014). Briefly, labeled RNA in RNA structure buffer (10 mM Tris pH = 7.0, 0.1 M KCl, 10 mM $MgCl_2$) was heated to 95 °C for 2 min, then left it at room temperature to allow proper secondary structure formation. Samples were subjected to RNA pull down using Pierce™ Magnetic RNA-Protein Pull-Down Kit (Thermo, 20164). The proteins were eluted and detected by immunoblotting analysis.

Mass spectrometry

1) In-Gel digestion

Gel section was cut into approx. 1 mm^3 pieces and destained using 30 mM $K_3Fe(CN)_6$:100 mM $Na_2S_2O_3$=1:1 solution. The reaction was stopped by removing supernatant, added 100 uL of 100 mM ammonium bicarbonate for 20 min, followed by dehydration in 100% acetonitrile for 5 min. Gel slice was then reduced by 20 mM DTT at 56 °C for 30 min and alkylated with 100 mM IAA at room temperate for 20 min. Gel slice was then incubated in a 50 mM ammonium bicarbonate solution containing 10 ng/mL trypsin (Promega Biotech Co., Madison, WI, USA.) overnight. Peptides were extracted with 0.1% TFA/80% acetonitrile, dried by vacuum centrifugation.

2) LC-MS/MS

The reverse phase high-performance liquid chromatography (RP-HPLC) separation was achieved on the Easy nano-LC system (Thermo Fisher Scientific) using a self-packed column (75 μm×150 mm; 3 μm ReproSil-Pur C18 beads, 120 Å, Dr.Maisch GmbH, Ammerbuch, Germany) at a flow rate of 300 nL/min. The mobile phase A of RP-HPLC was 0.1% formic acid in water, and B was 0.1% formic acid in acetonitrile. The peptides were eluted using a gradient (2–90% mobile phase B) over a 60 min period into a nano-ESI orbitrap Q Exactive mass spectrometer (Thermo Fisher Scientific). The mass spectrometer was operated in data-dependent mode with each full MS scan (m/z 300-1600) followed by MS/MS for the 10 most intense ions with the parameters: ≥ +2 precursor ion charge, 2 Da precursor ion isolation window and 27 normalized collision energy of HCD. Dynamic Exclusion™ was set for 45 s. The full mass and the subsequent MS/MS analyses were scanned in the Orbitrap analyzer with R = 70,000 and R= 17,500, respectively.

3) Data analysis

The MS data were analyzed using the software MaxQuant (http://maxquant.org/, version 1.6.5.0). Proteins were identified by searching MS and MS/MS data of peptides against an Mouse proteome database (downloaded from Uniprot). Trypsin/P was selected as the digestive enzyme with two potential missed cleavages. The search included variable modifications of methionine oxidation and N-terminal acetylation, and fixed modification of cysteine carbamidomethylation. Peptides of minimum 6 amino acids and maximum of two missed cleavages were allowed for the analysis. For peptide and protein identification, false discovery rate was set to 0.01.

Supplemental references

Fu, H., Wang, T., Kong, X., Yan, K., Yang, Y., Cao, J., Yuan, Y., Wang, N., Kee, K., Lu, Z.J., *et al.* (2022). A Nodal enhanced micropeptide NEMEP regulates glucose uptake during mesendoderm differentiation of embryonic stem cells. Nat Commun *13*, 3984. 10.1038/s41467-022-31762-x

Picelli, S., Faridani, O.R., Bjorklund, A.K., Winberg, G., Sagasser, S., and Sandberg, R. (2014). Full-length RNA-seq from single cells using Smart-seq2. Nat Protoc *9*, 171-181. 10.1038/nprot.2014.006

Wang, P., Xue, Y., Han, Y., Lin, L., Wu, C., Xu, S., Jiang, Z., Xu, J., Liu, Q., and Cao, X. (2014). The STAT3-binding long noncoding RNA lnc-DC controls human dendritic cell differentiation. Science *344*, 310-313. 10.1126/science.1251456

Zhao, B., Zhang, W.D., Duan, Y.L., Lu, Y.Q., Cun, Y.X., Li, C.H., Guo, K., Nie, W.H., Li, L., Zhang, R., *et al.* (2015). Filia Is an ESC-Specific Regulator of DNA Damage Response and Safeguards Genomic Stability. Cell stem cell *16*, 684-698. 10.1016/j.stem.2015.03.017